

NASA MEMO 1-3-59L

NASA MEMO 1-3-59L

NASA

1N 1-3-59L
374 570
p.

MEMORANDUM

MEASUREMENTS OF LOCAL HEAT TRANSFER AND PRESSURE ON
SIX 2-INCH-DIAMETER BLUNT BODIES AT A MACH NUMBER
OF 4.95 AND AT REYNOLDS NUMBERS
PER FOOT UP TO 81×10^6

By Morton Cooper and Edward E. Mayo

Langley Research Center
Langley Field, Va.

**NATIONAL AERONAUTICS AND
SPACE ADMINISTRATION**

WASHINGTON
March 1959

NATIONAL AERONAUTICS AND SPACE ADMINISTRATION

MEMORANDUM 1-3-59L

MEASUREMENTS OF LOCAL HEAT TRANSFER AND PRESSURE ON
SIX 2-INCH-DIAMETER BLUNT BODIES AT A MACH NUMBER
OF 4.95 AND AT REYNOLDS NUMBERS
PER FOOT UP TO 81×10^6

By Morton Cooper and Edward E. Mayo

SUMMARY

Measurements of the local heat transfer and pressure distribution have been made on six 2-inch-diameter, blunt, axially symmetric bodies in the Langley gas dynamics laboratory at a Mach number of 4.95 and at Reynolds numbers per foot up to 81×10^6 . During the investigation laminar flow was observed over a hemispherical-nosed body having a surface finish from 10 to 20 microinches at the highest test Reynolds number per foot (for this configuration) of 77.4×10^6 . Though it was repeatedly possible to measure completely laminar flow at this Reynolds number for the hemisphere, it was not possible to observe completely laminar flow on the flat-nosed body for similar conditions. The significance of this phenomenon is obscured by the observation that the effects of particle impacts on the surface in causing roughness were more pronounced on the flat-nosed body. For engineering purposes, a method developed by M. Richard Dennison while employed by Lockheed Aircraft Corporation appears to be a reasonable procedure for estimating turbulent heat transfer provided transition occurs at a forward location on the body. For rearward-transition locations, the method is much poorer for the hemispherical nose than for the flat nose.

The pressures measured on the hemisphere agreed very well with those of the modified Newtonian theory, whereas the pressures on all other bodies, except on the flat-nosed body, were bracketed by modified Newtonian theory both with and without centrifugal forces. For the hemisphere, the stagnation-point velocity gradient agreed very well with Newtonian theory. The stagnation-point velocity gradient for the flat-nosed model was 0.31 of the value for the hemispherical-nosed model. If a Newtonian type of flow is assumed, the ratio 0.31 will be independent of Mach number and real-gas effects.

INTRODUCTION

In recent years, the blunt reentry body has been the subject of extensive research, both experimental and theoretical. This research has been directed toward a better understanding of the flow so that more exact means for predicting and, hence, reducing the heat transfer to such bodies could be established. The problem of establishing the heat transfer to an arbitrary blunt body in axially symmetric flow usually divides into the study of two different flows: an external inviscid flow and a boundary-layer flow.

The status of the inviscid-flow problem (refs. 1 and 2) indicates that rapid progress has recently been accomplished in accurately predicting flow fields about blunt bodies with detached shocks. For several assumed shock shapes, the flow fields about corresponding bodies of physical interest have been computed. (See refs. 2 to 4.) In principle, therefore, if the proper shock shape can be deduced for an arbitrary body, the remainder of the flow field can be established. For the hemisphere, the experimental confirmation of the method outlined in reference 2 is excellent. In examining the comparisons shown in reference 2, it should be noted that for a Mach number of 5.8 the modified Newtonian theory would agree equally well. Hence, more experimental pressure information is required to establish the accuracy of the methods of references 2 to 4 for blunter bodies where such simplified procedures as the modified Newtonian theory are inadequate.

Once the external flow field has been established, the accuracy with which the heat transfer can be evaluated depends upon whether the boundary-layer flow is laminar or turbulent and upon when and where transition might occur. For the purely laminar-flow case, the method of reference 5 for the stagnation point coupled with the methods of references 6 and 7 predict, in general, the heat-transfer distribution around blunt bodies. For the turbulent-flow case, many choices of approximate methods exist (for example, refs. 8 to 10, with additional references in ref. 10, and a method developed by M. Richard Dennison while employed by the Missile Systems Division of Lockheed Aircraft Corporation in a paper not generally available), but the limits on each method have yet to be tangibly established. Hence, a reasonably reliable unified method for the turbulent-flow case is still lacking. In regard to the transition problem on blunt bodies, incompressible stability calculations (ref. 11) for a hemisphere indicate that, at least in the vicinity of the stagnation point, the boundary layer is stable for Reynolds numbers of practical concern. Whether this is the case for either subsonic or supersonic flow remains to be proved, inasmuch as data exist (for example, ref. 12) which indicate turbulent flow on blunt bodies. The quantitative influence of roughness on transition in these results (ref. 12) is unestablished.

The purpose of the present paper is to present the results of measurements of the local heat transfer and pressure distribution on six 2-inch-diameter, blunt, axially symmetric bodies in the Langley gas dynamics laboratory at a Mach number of 4.95 and at Reynolds numbers per foot ranging from 12×10^6 to 81×10^6 . Particular emphasis has been given to the results obtained on a hemispherical nose and on a flat nose.

SYMBOLS

A_n, C_n, n	arbitrary constants
a_t	stagnation-point speed of sound outside boundary layer
C_p	pressure coefficient, $\frac{p - p_\infty}{\frac{1}{2}\rho_\infty V_\infty^2}$
$C_{p,t}$	stagnation-point pressure coefficient, $\frac{p_t - p_\infty}{\frac{1}{2}\rho_\infty V_\infty^2}$
c_w	specific heat of model-skin material
D	base diameter of model
h	heat-transfer coefficient
k	local thermal conductivity outside boundary layer
M	nominal Mach number
M_l	local Mach number
M_{cl}	Mach number on jet center line
ΔM	incremental Mach number
N_{Nu}	Nusselt number, hs/k
N_{Pr}	Prandtl number
$N_{Re,D}$	free-stream Reynolds number, $\frac{\rho_\infty V_\infty D}{\mu_\infty}$
$N_{Re,s}$	local Reynolds number, $\frac{\rho us}{\mu}$

4

p	local pressure on model surface
P_t	stagnation-point pressure
$P_{t,\infty}$	free-stream stagnation pressure
p_∞	free-stream static pressure
R	base radius of model
R_h	radius of hemisphere model
r	radius of curvature of outer surface measured in plane including axis of symmetry, negative for convex bodies
s	distance along surface of model measured from stagnation point
T	temperature of model skin
T_r	recovery temperature
$T_{t,\infty}$	free-stream stagnation temperature
t	time
u	local velocity outside boundary layer
V_∞	free-stream velocity
x	distance parallel to axis of symmetry measured from stagnation point (fig. 1)
y	distance from axis of symmetry to outer surface of model (fig. 1)
z	dummy variable
γ	ratio of specific heats
δ	acute angle between axis of symmetry and tangent to outer surface
μ	local viscosity outside boundary layer
μ_∞	free-stream viscosity

ρ	local density outside boundary layer
ρ_t	stagnation-point density outside boundary layer
ρ_w	density of model-skin material
ρ_∞	free-stream static density
τ	skin thickness

APPARATUS, TESTS, AND METHODS

Jet

The tests were conducted in a 9-inch-diameter blowdown jet installed in the Langley gas dynamics laboratory. The circular nozzle was designed by the method of characteristics and the ordinates were corrected for boundary-layer growth by assuming a turbulent boundary layer. The calibrated Mach number in the test section is approximately 4.95 with a maximum deviation from this nominal value of about 0.04. The stagnation-pressure range of the jet when empty is 275 to 2,500 lb/sq in. with an atmospheric discharge. Stagnation pressures as low as approximately 50 lb/sq in. can be obtained by discharging into an existing vacuum system. The stagnation-temperature range of the jet is from about 0° F to 1,000° F; realistically, however, the lower temperature limit is set by condensation of oxygen in the nozzle. This occurrence imposes a lower limit of about 350° F at the higher pressures. Inasmuch as air to operate this jet is obtained from a 20,000-cubic-foot tank field at 5,000 lb/sq in., the duration of flow during a given test with atmospheric discharge can be very long, up to about 20 minutes, even at the highest pressures.

Models and Instrumentation

Geometry.- Six different nose shapes (fig. 1) were studied. These shapes included a hemisphere, a flat disk, and a family of four shapes having a prescribed Newtonian pressure distribution. The prescribed pressure distribution was arbitrarily specified as

$$\frac{p}{p_t} = 1 - C_n \left(\frac{s}{R} \right)^n$$

A pressure distribution of this form results in an increasingly favorable pressure gradient with distance. Furthermore, the choice of $n \geq 3$ establishes zero curvature at the stagnation point, a factor conducive

to low heat transfer. For the four models studied, the values of C_n were as follows:

$$\begin{array}{ll} C_3 = 0.597 & C_4 = 0.586 \\ C_3 = 0.356 & C_4 = 0.346 \end{array}$$

In each of the two general cases studied (that is, with n equal to 3 and 4), the larger of the C_n values corresponds to the vanishing of the pressure coefficient at the model base. For a given value of n , a lower value of C corresponds to a blunter body. (See fig. 1.) The derivation of the body shapes to satisfy the prescribed pressure distribution is outlined in appendix A.

Pressure models.- Pressure models of all six nose shapes (fig. 1) were tested. All models had a base diameter of 2 inches and orifices 0.015 inch in diameter. The orifices were located essentially in a vertical plane on the upper half of the model. In some instances it was necessary, for clearance purposes, to stagger the orifices slightly off the vertical plane. The pressure data were initially recorded on either laboratory-type gages or on a mercury manometer. During the data analysis of the blunter models, however, it became readily apparent that more precise measurements were required to establish the velocity gradients in the vicinity of the stagnation point for comparison of the heat-transfer data with theory. Accordingly, the flat-nosed model was retested and the difference between stagnation-point pressure and any other pressure along the body was recorded on a 10-foot butyl phthalate (specific gravity approximately equal to 1.04) manometer.

Heat-transfer models; $\tau = 0.030$ inch - Two separate sets of heat-transfer models were used. The first set consisted of all six shapes (though only four were tested, that is, models with $C_3 = 0.356$ and $C_4 = 0.346$ were not tested) and had a nominal skin thickness of 0.030 inch. The actual thickness of each model varied from stagnation point to base, with the variation amounting to 0.015 inch in the worst case. Hereinafter, this set will be designated as the 0.030 models. The construction details of these models were of an exploratory nature. The models consisted of a thin skin of type 303 stainless steel supported on three pins located 120° apart near the outer edge of the skin. These pins connected the skin to the sting support. Chromel-alumel thermocouples, the outputs of which were recorded on an 18-channel galvanometer, were spot-welded to the inner surface of the skin and were located on the top half of the model in the plane of symmetry. After the thermocouples were installed, the interiors of the models, between the skin and sting, were filled with an insulating composition consisting primarily of a light earthen material to which an additive had been mixed in order

to harden the fill material. The fill material was required to support the thin shells which were subjected to external pressures in excess of 150 lb/sq in. Unfortunately, heat transfer to the fill material, as discussed in reference 13, had a significant effect on lowering the apparent heat-transfer data. Based on rough estimates of the thermal conductivity and specific heat of the fill material, the heat-transfer data were lowered from perhaps 10 to 20 percent with the amount depending on the heat-transfer coefficient; that is, the larger the coefficient, the larger the error. The magnitude of this drop was substantiated qualitatively by means of tests of two additional models as will be discussed subsequently. Because of the uncertainty of the thermal conductivity of the fill material as well as the uncertainty of contact resistance between the skin and the fill material, no attempt has been made to correct the data. Hence, the data for the 0.030 models will be used solely to establish the location of transition and for comparative purposes which would be little affected by the fill-material problem.

The surface finish of these models was estimated by means of an interference microscope. In general, at the start of the test program the models had a background finish between 2 and 5 microinches, but in all cases there were extensive polishing scratches between 10 and 20 microinches. In addition, a significant amount of pitting of the surface occurred during each test from impacts of particles in the airstream with the model surface. In order to minimize the effects of these pits, which were between 0.002 and 0.005 inch in diameter, the models were polished between tests to eliminate high spots and sharp edges around the pits. No accurate measurements of the depth of the pits were made.

Heat-transfer models; $\tau = 0.060$ inch.- The second set of heat-transfer models used consisted of two nose shapes, a flat nose and a hemispherical nose, and had a nominal skin thickness of 0.060 inch. Hereinafter, this set will be designated as the 0.060 models. These models were designed and constructed after the tests of the 0.030 models were completed and the data partially analyzed. The skin thickness of 0.060 inch was selected as a compromise between structural and data-reduction requirements. No fill material was used, and a vacuum was maintained inside the models during the tests to eliminate the fill-material problem. The contour of the new hemispherical-nosed model extended beyond the 90° station. (See the dashed region in fig. 1.) For these models thermocouples were installed by drilling two small holes normal to the model and pushing each lead of the thermocouple into a separate hole. The holes were then filled with a material having approximately the same product of density and specific heat as that of the skin. The thermocouples were spiraled around the hemisphere; whereas they alternated on each side of a vertical plane on the flat-nosed model.

Both of the 0.060 models were made of 17-4 PH stainless steel and were hardened after machining to resist abrasion better. For these models a background finish of about 2 microinches existed before the first tests.

However, as in the case of the 0.030 models, there was extensive coverage of scratches between 10 and 20 microinches. These scratches, by virtue of the polishing procedure, were undoubtedly depressions in the surface. For these 0.060 models there was no polishing between tests with the result that the models became rougher with each test.

Installation

In general, two separate installations were used (fig. 2) - a fixed support for the pressure models (fig. 2(a)) and a "push-in" side support (figs. 2(b) and 3) for the heat-transfer models. The pressure models were tested first. Difficulties in starting the jet with these blunt bodies would not permit the use of the side support with the model installed prior to the establishment of supersonic flow. (See fig. 2(b) for installed location.) However, it was possible to make the pressure tests with the rather unorthodox support shown in figure 2(a).

For the heat-transfer tests the problem of starting the jet was eliminated by increasing the area of the second minimum and by inserting the model into the test section after supersonic flow was established at the proper stagnation conditions. In order to insert the model into the jet, a vertical door (fig. 3) was lowered by means of a pneumatic cylinder. During the lowering process, air induced from the room choked the jet. When the vertical door was fully retracted, it triggered the push-in cylinder (fig. 3) which inserted the model into the test section in less than 0.1 second. Flow was reestablished almost immediately. In order to minimize model pitting, the jet was shut down as soon as data were obtained.

The repeat test of the flat-nosed pressure model using the butyl phthalate manometer was made (after completion of the heat-transfer tests) by using the heat-transfer support and the test procedure for inserting the heat-transfer model.

Test Conditions

Pressure models.- The free-stream Mach number for all tests was 4.95. For the initial set of pressure tests of the models, the stagnation pressure ranged from a nominal value of 600 to 2,500 lb/sq in. at a stagnation temperature of approximately 375° F. For the repeat tests of the flat-nosed model using the butyl phthalate manometer, the stagnation pressure ranged from 400 to 1,500 lb/sq in., though it should be noted that a pressure of about 1,500 lb/sq in. was required to start the jet. For the pressure tests the free-stream Reynolds number ranged from 12.2×10^6 to 76.3×10^6 per foot or from 2.0×10^6 to 12.7×10^6 based on body diameter. The specific conditions for each test are presented in tables I and II.

Heat-transfer models.- In the heat-transfer tests of the models, the stagnation pressure was varied from 1,000 to 2,500 lb/sq in., and the stagnation temperature was either 400° F or 700° F. The free-stream Reynolds number ranged from 18.5×10^6 to 72.5×10^6 per foot or from 3.1×10^6 to 12.1×10^6 based on body diameter. The specific conditions for each test are specified in tables III and IV. With the exception of one data point (which was obtained 0.7 second after obtaining the other data for reasons discussed subsequently), all heat-transfer data presented were obtained about 0.4 second after the model was inserted into the airstream. When the data were obtained, the model surface was essentially isothermal at roughly 110° F for the 400° F tests and at 150° F for the 700° F tests. These temperatures correspond to wall-to-stream stagnation-temperature ratios of 0.66 and 0.53, respectively, ratios which are representative of the entire test program.

Data Reduction

Pressure models.- For the pressure models all data have been non-dimensionalized in terms of the stagnation-point pressure. The flow variables outside the boundary layer (required in the heat-transfer analysis) have been evaluated from the measured pressures and the assumption of isentropic flow behind the shock wave. Because any Reynolds number effects on the pressure distributions were within the limits of accuracy of the results, a single curve was faired through all pressure data for a given model and was used in evaluating the flow conditions outside the boundary layer. In computing the velocity in the vicinity of the stagnation point on the flat-nosed model, the formula

$$u = \sqrt{\frac{2(p_t - p)}{\rho F_c}} \quad (1)$$

was used in order to retain numerical accuracy in the data reduction. The value of F_c can be obtained from the relation

$$F_c = \frac{2}{\gamma M_l^2} \left[\left(1 + \frac{\gamma - 1}{2} M_l^2 \right)^{\frac{\gamma}{\gamma - 1}} - 1 \right]$$

or, in its more usual expanded form, from

$$F_c = 1 + \frac{1}{4} M_l^2 + \frac{1}{40} M_l^4 + \dots \quad (M < \sqrt{5})$$

In the vicinity of the stagnation point ($M_1 < 0.2$ or $\frac{p_t - p}{p_t} < 0.028$), the product ρF_c can be replaced by ρ_t with an error of less than 0.5 percent in velocity. Experimental velocity gradients were established graphically.

Heat-transfer models.- The heat-transfer data for the models were evaluated by means of the calorimeter technique. The heat entering the front face of the model was equated to the heat stored in the model by assuming that lateral conduction, the temperature difference across the skin, and radiation are negligible. For such a case, the heat balance for a thin, axially symmetric shell of arbitrary profile and constant thickness is

$$h = \frac{\rho_w c_w \tau}{T_r - T} \frac{dT}{dt} \left(1 - \frac{\tau \cos \delta}{2y} \right) \left(1 + \frac{\tau}{2r} \right) \quad (2)$$

where the radius of curvature r is negative for convex bodies. The terms in parentheses in equation (2) are simply geometric corrections accounting for the difference in surface area of the inner and outer surfaces. For a hemisphere,

$$\frac{\cos \delta}{y} = \frac{1}{R_h}$$

Hence, by neglecting the square of τ/R_h , the heat-transfer coefficient in equation (2) can be written for the hemisphere as

$$h = \frac{\rho_w c_w \tau}{T_r - T} \frac{dT}{dt} \left(1 - \frac{\tau}{R_1} \right) \quad (3)$$

since the thickness is small compared with the radius. For the flat disk, the heat-transfer coefficient in equation (2) becomes

$$h = \frac{\rho_w c_w \tau}{T_r - T} \frac{dT}{dt} \quad (4)$$

In order to evaluate the limitations on the data imposed by equations (2) to (4), the effects of the approximations must be considered. Computed lateral conduction and radiation losses were completely negligible inasmuch as the model was essentially isothermal at wall temperatures of about 150° F or less. In order to evaluate the effect of the temperature difference across the skin resulting from the finite thermal conductivity of the skin, the response of a thermocouple located on the inner skin surface to a heating rate proportional to the difference in recovery temperature and outer skin temperature was computed from a

solution of the one-dimensional, unsteady, heat-flow equation. (See ref. 14.) From this calculation, the output of the inner surface thermocouple was compared with the true heat-transfer coefficient given as a boundary condition. A correction factor directly applicable to the data was determined. This correction factor amounted to an increase in h as given by equations (2) to (4) by as much as 8 percent at maximum and was applied to the 0.060 models. In general, the increase was much less. The correction amounted to less than 4 percent for the 0.030 models and was not applied because of the previously discussed limitation on the 0.030-model data. This general problem of the effects of finite thermal conductivity and fill material on composite one-dimensional slabs has been recently treated in reference 15.

No attempt was made to measure the recovery temperature because for blunt-nosed models the recovery temperature does not deviate much from the stagnation temperature. Furthermore, if the models were to remain in the flow sufficiently long to establish recovery temperatures, pitting due to fine-particle impacts on the surface would roughen the models, cause transition, and invariably result in turbulent-flow recovery temperatures. Hence, the recovery temperatures were computed based on either the square root or cube root of the Prandtl number (by using local conditions outside the boundary layer) with the choice depending on whether the data were laminar or turbulent. In all cases, the actual choice is indicated in tables III and IV. For extreme cases, as indicated in tables III and IV, the results, in general, are little affected by the choice used in establishing the recovery factor.

RESULTS AND DISCUSSION

Pressure Models

Pressure distributions.- Representative pressure distributions are summarized in figure 4 and table I where the local pressure (expressed as a fraction of stagnation-point pressure) is presented as a function of nondimensional arc length. Also shown in figure 4 are calculations for modified Newtonian theory and modified Newtonian theory plus centrifugal forces. (See ref. 16.) In applying modified Newtonian theory in which

$$\frac{C_p}{C_{p,t}} = \sin^2 \delta$$

the difference between pressure and pressure coefficient has been retained so that in figure 4

$$\frac{p}{p_t} = \sin^2 \delta + \frac{p_\infty}{p_t} \cos^2 \delta$$

For the flat-nosed model, Newtonian flow is trivial and yields stagnation-point pressure across the nose. For this body, the approximate theoretical estimate given in figure 5 of reference 17 is presented.

For the hemispherical-nosed model, the comparison of experiment with Newtonian theory shows excellent agreement. This type of agreement is characteristic of nearly hemispherical bodies. (See ref. 1.) In fact, for the hemisphere, previous tests (refs. 13 to 23) have indicated similar agreement over a wide Mach number range from below 3 to about 8 for a wide Reynolds number range. Those small deviations that do exist over the Mach number and Reynolds number range tend to indicate that the data are slightly low with respect to theory.

For the blunter C_n bodies, the disagreement becomes very evident. Unfortunately, more exact calculations made by the methods of references 2 and 3 are not available for these cases where Newtonian theory is found lacking. In figure 4, the data are seen to be bracketed by the Newtonian theory both with and without centrifugal forces. It is of limited interest to note that, if the maximum value of the centrifugal correction is restricted to that value occurring at a pressure ratio of about 0.9 (empirical curve), rather good agreement is obtained with these data.

The pressure on the flat-nosed model (fig. 4) is in close agreement with similar results obtained at $M = 4.76$ and reported in reference 24. In addition, the results are consistent with the calculations of reference 17 for the range shown. However, quantitative limitations on the numerical calculations (as pointed out in ref. 17), together with the rather compressed scale for the flat-nosed pressures (fig. 4), limit the significance of the comparison.

In an attempt to assess overall limitations on the measurement of blunt-body pressure distributions and, consequently, velocity distributions (see eq. (1)), a much more detailed program was undertaken to study the flat-nosed model. The results are presented in figure 5 in which the changes in pressure from the stagnation-point value have been amplified by a factor of 50 from those in figure 4. These measurements, made by using the butyl phthalate manometer,^a have been presented for the following conditions:

(1) Model located on jet center line with orifices in a vertical plane both above (up) and below (down) the jet center line (fig. 5(a))

(2) Model located 1 inch from the jet center line with orifices in a vertical plane both above and below the jet center line (fig. 5(b))

^aIt is significant to note that, at a stagnation pressure of 1,500 lb/sq in., the stagnation-point pressure is 94 lb/sq in. and the maximum pressure difference for the data shown in figure 5 is only 2.2 lb/sq in.

(3) A calibration of the jet with total-pressure tubes located to correspond exactly with the orifice-up condition of figure 5(a) (fig. 5(c))

Ideally, the flat-nosed-model pressure data shown for the four different sets of orifice locations in figures 5(a) and 5(b) should be identical. Actually, the spread is not very large, and the choice of a mean value of each set of data would bring all the data into good agreement. For all subsequent calculations, the orifice-up configuration with the model located 1 inch from the jet center line (fig. 5(b)) will be treated as the proper flat-nosed-model distribution because this distribution varies least with pressure and because it would be an excellent mean of all other data. However, the extreme curves of figure 5 correspond to a spread of about 20 percent in stagnation-point velocity gradient, a subject which will be considered subsequently in more detail. Though the free-stream variations in the jet are small (fig. 5(c)), they are of the same magnitude as the body induced pressure field. For such a condition, which is unusual in model testing, it becomes exceedingly difficult to assess the accuracy of the results.

Velocity and velocity gradients.- One of the prime purposes in measuring the pressures on blunt bodies is to establish the velocity and velocity gradients for heat-transfer calculations. The velocities calculated from the pressure measurements of figures 4 and 5 are presented in figures 6 and 7, respectively. In these plots, distances have been nondimensionalized in terms of the model base radius and velocities have

been nondimensionalized in terms of $\sqrt{1.4 \frac{p_t}{\rho_t} \left(1 - \frac{p_\infty}{p_t}\right)}$. For an ideal gas and a Mach number reasonably high for p_∞/p_t to be negligible,^b this parameter is the stagnation speed of sound. The reasons for the choice of this nondimensionalizing velocity are discussed in appendix B. Of course, the distinction between the stagnation speed of sound and $\sqrt{1.4 \frac{p_t}{\rho_t}}$ has meaning only when results such as these are applied to conditions in which real-gas effects exist. Then, as pointed out in appendix B, the use of the real-gas speed of sound at the stagnation point, a common procedure, would result in the underestimation of the velocity gradient by a maximum of 13 percent from that predicted by using $\sqrt{1.4 \frac{p_t}{\rho_t}}$, a parameter which can be justified by Newtonian considerations.

A comparison of the experimental and Newtonian theoretical velocity distributions for all shapes except the flat (for which no theory is presented) shows, in general, good agreement. For the hemisphere, the agreement is excellent as indicated previously in figure 4 for the pressures.

^bFor $M = 5.0$, the value of p_∞/p_t is 0.031 for an ideal gas.

For the other models, the theory tends to be low. The detailed velocity distributions for the flat-nosed model (fig. 7) reflect the effects of model location and jet stagnation pressure which were previously shown for the pressure distributions in figure 5.

The velocity-gradient curves for the C_n bodies and the hemisphere are compared with Newtonian theory in figure 6. A comparison of Newtonian theory with the flat-nose results is trivial since Newtonian theory predicts zero gradient for zero curvature. Again the results for the hemisphere indicate excellent agreement with theory up to a value of s/R of at least 0.9 at which point the theory overestimates the data. For the C_n bodies the agreement is very good except in the immediate vicinity of the stagnation point where the curvature is exceedingly small and Newtonian theory fails. In each case for the C_n bodies the location where the theory markedly diverges from the experiment corresponds to a local radius of curvature that is roughly twice that of the model base radius.

For the flat-nosed model, the representative data of figure 6 and the detailed data of figure 7 indicate a constant velocity gradient from the stagnation point to a value of s/R of about 0.5. The best estimate of this velocity-gradient parameter on the basis of these data is given by

$$\frac{R}{\sqrt{1.4 \frac{p_t}{\rho_t} \left(1 - \frac{p_\infty}{p_t}\right)}} \frac{du}{ds} = 0.375$$

As previously pointed out, however, a maximum spread of 20 percent (± 10 percent) exists in the extreme measured values, a spread which is believed to be associated with jet conditions. A comparison of the value 0.375 with the data at $M = 2.01$ and $M = 4.76$ on a flat nose in reference 24 (data in which there are apparently accuracy problems, also) indicates that the present value agrees with the average of the results obtained at $M = 2.01$ and $M = 4.76$. The scatter of the three values of the velocity gradient with Mach number, however, again points out the limitations on experimental velocity determinations on blunt-nosed bodies. If a Newtonian type of flow were to exist, all three velocity-gradient measurements should be the same because the parameter compared is independent of Mach number. (See appendix B.)

In order to assess the "effective" velocity method of establishing the velocity gradients on very blunt bodies (ref. 25), the incompressible-flow stagnation-point velocity gradients for the hemisphere and flat nose (ref. 26^c) are shown in figure 6. These values have been computed by

^cThe flat-nose velocity gradient was derived from the planetary ellipsoid solution given in reference 26.

assuming that free-stream velocity corresponds to the velocity behind the model bow shock. Since Newtonian theory predicts the flow in the vicinity of the hemisphere stagnation point so well, an effective velocity correction is obtained for the hemisphere from the ratio of the Newtonian gradient to the incompressible-flow gradient. This effective velocity correction is then assumed to apply to the incompressible flow about other blunt bodies. As can be seen from figure 6, such a procedure overestimates the flat-nosed-model velocity gradient by more than 25 percent.

The ratio of the stagnation-point velocity gradient of the flat-nosed model to that of the hemispherical-nosed model is 0.31; thus, the corresponding ratio of heat-transfer coefficients would be anticipated to be 0.56 based on laminar-flow theory.

The problem of estimating the velocity gradients in the vicinity of stagnation points of very blunt bodies, such as the C_n bodies, still remains a subject for further study. A lower limit can be obtained by superposing the experimental flat-nosed-model distribution on the calculated Newtonian distribution for the shape being considered. The higher value of the two curves will give a lower limit to the velocity gradient in the region of the stagnation point; the estimate should improve with distance from the stagnation point. A further improvement in estimating the stagnation-point velocity gradient can be made by using stagnation-point correlation procedures such as those presented in reference 24.

Heat-Transfer Models

The heat-transfer data for the 0.030 and 0.060 models are presented in figures 8 and 9, respectively, and in tables III and IV, respectively. For the 0.060 models, both heat-transfer coefficient and $N_{Nu}/\sqrt{N_{Re}}$ are presented; for the 0.030 models, only heat-transfer coefficients are presented because the significance of the laminar correlating parameter $N_{Nu}/\sqrt{N_{Re}}$ becomes questionable because of heat flow into the fill material.

Hemisphere model.- The most significant result of these tests was the attainment of laminar flow over the complete hemisphere (figs. 8 and 9(a)) at the highest possible test Reynolds number. For the 0.030 hemisphere (fig. 8), this result occurred at a Reynolds number of 12.9×10^6 based on body diameter or a unit Reynolds number of 77.4×10^6 per foot. For the 0.060 hemisphere (fig. 9(a); test 56), this result occurred at Reynolds numbers of 12.1×10^6 based on body diameter and 72.6×10^6 per foot. Proof of the existence of laminar flow is more clearly evident in figure 9(a) where data are shown for successive tests. The first test at 2,500 lb/sq in. (see circular-

shaped symbols) is, with the exception of one data point, completely below the laminar-flow theory of reference 19. Reference 19 has been used in preference to reference 6 for these tests because deviations from ideal-gas values are small in the range of the present tests. The theory has been computed by using experimental pressures; however, in view of the previously established agreement between experimental and theoretical pressures, the theoretical curve would be little affected by the use of Newtonian pressures. The data are considerably below that of the theory (ref. 19) by about 15 percent at the stagnation point for tests 56 and 57. Uncertainty in the determination of the skin thickness can account for 5 percent of this discrepancy at most. The use of a Sutherland viscosity variation (ref. 27), in place of the linear variation used in reference 19, has only a slight effect on the theoretical stagnation-point heat-transfer value. Though the discrepancies in some cases are very large, it is reasonably clear that the flow is laminar for test 56. This can be further substantiated by considering the solid circular-shaped symbol ($\frac{s}{R} = 1.05$; fig. 9(a)) which was obtained 0.7 second after obtaining the other data presented for this test. The solid symbol denotes a discontinuous change in the galvanometer record which indicates the occurrence of transition which was caused by impacts of particles in the airstream with the model surface. At subsequent times during this same test, other thermocouples also indicated considerably higher heat-transfer rates. At the conclusion of the test the model surface was found to contain discrete pits from 0.002 to 0.003 inch in diameter. The model was then retested without polishing (test 57; square-shaped symbols). The effects of the surface roughness are apparent; transition occurred at a value of s/R of approximately 0.35. In the next test (test 58; diamond-shaped symbols), which was made without model polishing and at a reduced stagnation pressure, transition shifted rearward to a value of s/R of approximately 1.0.

The heat-transfer data have been compared with the method of Dennison for a Prandtl number of 0.7 and 1.0. Conclusions drawn from this comparison must be related to the transition-point location, inasmuch as the method of Dennison assumes a fully turbulent flow starting from the stagnation point. By using the curve with a Prandtl number of 0.7 as a standard, the data agree in magnitude with the calculations but are shifted to higher values of s/R . If transition had occurred more forward on the body, the agreement would probably be very good. The fact that the data point indicated by the solid symbol from test 56 is considerably lower than the corresponding data point from test 57 is attributed to transition occurring more rearward initially. For a stagnation pressure of 1,000 lb/sq in. (test 58), Dennison's method would be considerably in error because of the rearward location of transition. The data for the 0.030 hemisphere (fig. 8), subject to the previously discussed restrictions, are compatible with the laminar heat-transfer data for the 0.060 hemisphere.

The extremely high Reynolds number of 12.9×10^6 for transition-free flow on a hemisphere is one of the highest observed to date. If the surface-finish scratches from 10 to 20 microinches coupled with the extremely thin boundary layer associated with the unit Reynolds number of 77.4×10^6 are considered, this result (obtained in a blowdown jet) is even more surprising. The establishment of the existence of laminar flow for such an extreme Reynolds number condition was possible only because the heat-transfer data could be obtained almost immediately upon exposure of the model to the airstream and prior to transition caused by particle impacts on the model surface.

C_n models.- The heat-transfer data for the C_n models (fig. 8) indicate such close similarity between $C_3 = 0.597$ and $C_4 = 0.586$ for stagnation conditions of 1,000 lb/sq in. and 400° F that no further tests were conducted for $C_3 = 0.597$. Rather complete data, however, were obtained and are presented for $C_4 = 0.586$. For orientation purposes in a plot of this sort, the heat-transfer coefficient would be expected to vary as the square root of the stagnation pressure and approximately as the fourth root of the stagnation temperature according to laminar-flow theory. From the shape of the curves the three lower curves for $C_4 = 0.586$ apparently correspond to laminar flow over the complete body; the two upper curves indicate transition beginning in the vicinity of a value of s/R of 0.4. It is possible only to speculate as to the relative importance of roughness in causing transition on this model; however, in this speculation the following information should be noted. The $C_4 = 0.586$ model was polished between tests but the particle-impact problem was considerably more severe for the stagnation condition at 700° F than for the stagnation condition at 400° F. Hence, though transition is indicated only for the two highest Reynolds numbers in non-consecutive tests, it is not unlikely that transition is caused by roughness. Such an occurrence is possible because, for the lower Reynolds number (7.9×10^6) and thicker boundary layer, the stagnation temperature was 700° F and, therefore, pitting was a more severe problem. For the higher Reynolds number (12.9×10^6), the boundary layer was thinner and, consequently, was more susceptible to the presence of a given amount of roughness.

Flat-nosed models.- The data for the 0.060 flat-nosed model (fig. 9) indicate early transition for all three tests.^d The proof of the existence of turbulent flow stems from a comparison of these data with both laminar- and turbulent-flow calculations or from a comparison of these data with the turbulent-flow curve for $C_4 = 0.586$ at the highest

^dIf transition were caused by roughness during the first test, its occurrence during subsequent tests is not very significant inasmuch as there was no polishing between tests.

Reynolds number. If allowance is made for the lower heating level of $C_4 = 0.586$, the data show consistent trends up to a value of s/R of at least 0.8. A comparison of the flat-nosed-model data with theory indicates that the data are considerably above the laminar curve and are in reasonable agreement with Dennison's method for a Prandtl number of 0.7 rearward of the stagnation region. This agreement with turbulent-flow theory is enhanced by a somewhat fortuitous location of the transition point. Of course, from the general shapes of the laminar and turbulent heating curves, the location of transition would not be as critical in affecting the accuracy of the turbulent-flow estimate for the flat-nosed model as for the hemispherical-nosed model.

At 2,500 lb/sq in. the data obtained on the 0.030 model are compatible with that on the 0.060 model, though in all cases the heat transfer at the stagnation point of the 0.030 model is low. Laminar flow, as evidenced by the essential constancy of the heat-transfer coefficient up to a value of s/R of 0.75, was obtained on the flat-nosed model (fig. 8) during only one test (see square-shaped symbols) at a Reynolds number of 7.7×10^6 .

The stagnation-point heat-transfer data (fig. 9) are approximately 10 percent greater than theoretical values. Although this increase is probably an accuracy limitation on the heat-transfer data, it should be noted that, if the effects of roughness on the laminar heat transfer to a stagnation point reported in reference 22 can be extrapolated to the present tests, the surface finish from 10 to 20 microinches would be enough to account for the 10-percent increase. Of course, it is easily argued that such an increase was not manifested for the hemisphere.

Comparison of hemispherical- and flat-nosed models.— The measured velocity gradients at the stagnation points indicate, according to laminar-boundary-layer theory, that the ratio of stagnation-point heat-transfer of the flat nose to that of the hemispherical nose is 0.56. Experimentally, the measured ratio is about 0.7. The discrepancy between the two numbers is a cumulative effect (fig. 9); the value of the hemisphere is less than that of the theory and the value of the flat-nosed model is higher than that of the theory. On the basis of the relative difficulties and precision limits for these particular tests, the ratio 0.56 is considered more reliable.

As regards the transition problem, it was repeatedly possible to obtain completely laminar flow to the highest possible test Reynolds numbers for the hemisphere. It was never possible to obtain completely laminar flow on the flat-nosed model for similar conditions. The significance of this phenomenon is obscured by the observation that the effects of particle impacts on the surface in causing roughness were more pronounced on the flat-nosed model.

CONCLUDING REMARKS

Measurements of the local heat transfer and pressure distribution have been made on six 2-inch-diameter, blunt, axially symmetric bodies in the Langley gas dynamics laboratory at a Mach number of 4.95 and at Reynolds numbers per foot up to 81×10^6 . During the investigation laminar flow was observed over a hemispherical-nosed body having a surface finish from 10 to 20 microinches at the highest test Reynolds number per foot (for this configuration) of 77.4×10^6 . However, surface roughness caused by small particles in the airstream quickly established transition forward on the hemisphere. Though it was repeatedly possible to measure completely laminar flow up to the highest possible test Reynolds number for the hemisphere, it was not possible to observe completely laminar flow on the flat-nosed body for similar conditions. The significance of this phenomenon is obscured by the observation that the effects of particle impacts on the surface in causing roughness were more pronounced on the flat-nosed model. The determination of the existence of turbulent flow on the flat-nosed model was more difficult than on the hemispherical-nosed model because the change in heating level as a result of transition is not as pronounced. For engineering purposes, a method developed by M. Richard Dennison while employed by Lockheed Aircraft Corporation appears to be a reasonable procedure for estimating turbulent heat transfer provided transition occurs at a forward location on the body. For rearward-transition locations, the method is much poorer for the hemisphere than for the flat-nosed model.

The pressures measured on the hemisphere agreed very well with modified Newtonian theory, whereas the pressures on all other bodies, except on the flat-nosed body, were bracketed by modified Newtonian theory both with and without centrifugal forces. For the hemisphere, the stagnation-point velocity gradient agreed very well with Newtonian theory. The stagnation-point velocity gradient for the flat-nosed model was 0.31 of the value for the hemispherical-nosed model. If a Newtonian type of flow is assumed, the ratio 0.31 will be independent of Mach number and real-gas effects.

Langley Research Center,
National Aeronautics and Space Administration,
Langley Field, Va., October 1, 1958.

APPENDIX A

DERIVATION OF SHAPE OF BLUNT-NOSED BODY HAVING
A PRESCRIBED PRESSURE DISTRIBUTION

If the pressure distribution along a body is specified as

$$\frac{p}{p_t} = 1 - C_n \left(\frac{s}{R}\right)^n \quad (A1)$$

where C_n and n are arbitrary constants, the shape of the body can be established if the aerodynamic relationship between the pressure and body shape is known. If it is assumed that the external flow field as given by modified Newtonian flow is

$$\frac{C_p}{C_{p,t}} = \sin^2 \delta \quad (A2)$$

equations (A1) and (A2) can be combined with the geometric relation

$$\cos \delta = \frac{dx}{ds}$$

to obtain the distance along the surface as a function of x . Thus,

$$\frac{s}{R} = \frac{n+2}{2} A_n \left(\frac{x}{R}\right)^{\frac{2}{n+2}} \quad (A3)$$

where^a

$$A_n = \left(\frac{2}{n+2}\right)^{\frac{n}{n+2}} \left(\frac{1 - \frac{p_\alpha}{p_t}}{C_n}\right)^{\frac{1}{n+2}}$$

The equation for the body shape is obtained by differentiating $s(x)$ as given by equation (A3) with respect to x , and then by replacing the differential arc length by Cartesian differentials. In integral form the equation of the body shape is

^aThough C_n is an arbitrary constant and it is unnecessary to retain the term p_α/p_t in the definition of A_n , it was retained in the bodies derived for this investigation.

$$\frac{y}{R} = \frac{n+2}{2n} A_n \int_0^{\frac{x}{R}} \frac{\left(\frac{x}{R}\right)^{\frac{2n}{n+2}} \left(1 - \frac{z}{A_n^2}\right)^{1/2}}{z^{\frac{n-1}{n}}} dz \quad (\text{A4})$$

For $n > 2$, closed integration of equation (A4) was not possible. However, since $0 \leq \frac{z}{A_n^2} \leq 1$, the integrand can be expanded into a series. Integrating this series termwise yields the body shape as

$$\frac{y_n}{R} = \frac{n+2}{2} A_n \left(\frac{x}{R}\right)^{\frac{2}{n+2}} \left[1 - \frac{1}{2(n+1)} \frac{1}{A_n^2} \left(\frac{x}{R}\right)^{\frac{2n}{n+2}} - \frac{1}{8(2n+1)} \frac{1}{A_n^4} \left(\frac{x}{R}\right)^{\frac{4n}{n+2}} - \frac{1}{16(3n+1)} \frac{1}{A_n^6} \left(\frac{x}{R}\right)^{\frac{6n}{n+2}} - \dots \right] \quad (\text{A5})$$

Equation (A5) was used to compute the body shapes. The rapidity of convergence of the solution was established by comparing the coordinates given by equation (A5) with the exact coordinates computed for $n = 2$ from

$$\frac{y_2}{R} = A_2^2 \left[\sqrt{\frac{x}{A_2^2 R} \left(1 - \frac{x}{A_2^2 R}\right)} + \frac{\pi}{4} + \frac{1}{2} \sin^{-1} \left(\frac{2x}{A_2^2 R} - 1 \right) \right] \quad \left(-\frac{\pi}{2} \leq \sin^{-1} z \leq \frac{\pi}{2} \right) \quad (\text{A6})$$

The maximum difference between values of y_2/R as computed from equations (A5) and (A6) was less than 1 percent when the maximum value of $x/A_2^2 R$ was used for $A_2 = 1.0$. For $n > 2$, the convergence of the series in equation (A5) would be more rapid. In addition, the pressure distributions computed by differentiating equation (A5) were compared with the design requirements given in equation (A1). The differences for the range of variables compared in figure 4 were hardly noticeable.

APPENDIX B

APPLICATION OF IDEAL-GAS VELOCITY MEASUREMENTS
TO REAL-GAS HEAT-TRANSFER CALCULATIONS

In order to compute the real-gas heat transfer at a stagnation point (ref. 5), evaluation of the real-gas stagnation-point velocity gradient is necessary.^a Unfortunately, no real-gas measurements of the velocity gradient have been attempted because of the experimental complexities of this problem. Instead, theory or ideal-gas measurements (such as those of the present investigation) have been used. When a theory such as the modified Newtonian theory is used, the computations are straightforward. (For example, see ref. 5.) However, when experimental results or perhaps ideal-gas calculations (refs. 2 and 3) must be used, a question arises as to the proper method for extrapolating ideal-gas velocity measurements for real-gas application. One possible means for this extrapolation would be to use Newtonian theory as a guide for the determination of suitable nondimensionalizing parameters; for example, by using Newtonian theory the velocity gradient at the stagnation point is given by

$$\frac{du}{ds} = -\frac{1}{r} \sqrt{\frac{2p_t}{\rho_t} \left(1 - \frac{p_\infty}{p_t}\right)} \quad (B1)$$

or by

$$\frac{R}{\sqrt{1.4 \frac{p_t}{\rho_t} \left(1 - \frac{p_\infty}{p_t}\right)}} \frac{du}{ds} = -\frac{R}{r} \sqrt{\frac{2}{1.4}} \quad (B2)$$

The form of the nondimensionalized velocity gradient on the left side of equation (B2) is used throughout the report. Essentially the same parameter, aside from arbitrary constants, is used in reference 24. (The right-hand side of eq. (B2) is assumed to be given by experiment or by an ideal-gas theory.) The velocity gradient has been nondimensionalized in terms of the base radius of the model, rather than in terms of the radius of curvature at the stagnation point, to simplify application to a body with zero curvature. The constant 1.4 has been introduced arbitrarily to make the nondimensionalizing velocity equal to the

^aIn this discussion the velocity gradient at the stagnation point will be used as an illustration; the results generalize to other velocity parameters.

stagnation-point speed of sound for an ideal gas at high Mach numbers (with p_∞/p_t being negligible). The quantity $\sqrt{1.4 \frac{p_t}{\rho_t}}$ is not the stagnation-point speed of sound for air at high temperatures, though it is a fair approximation. For air at high temperatures the speed of sound is given by

$$a_t^2 = \frac{p_t}{\rho_t} f$$

where the function f , according to reference 28, is in the range $1.1 \leq f \leq 1.4$ for temperatures up to $11,000^\circ \text{K}$ and pressures ranging from 10^{-4} to 10^2 atmospheres. Hence,

$$1 \leq \frac{\sqrt{1.4 \frac{p_t}{\rho_t}}}{a_t} \leq 1.13$$

From this limiting relationship, it is established that using the real-gas stagnation-point speed of sound would underestimate the velocity gradient by a maximum of 13 percent from that predicted by using the

quantity $\sqrt{1.4 \frac{p_t}{\rho_t}}$ for high Mach numbers.

REFERENCES

1. Lees, Lester: Recent Developments in Hypersonic Flow. *Jet Propulsion*, vol. 27, no. 11, Nov. 1957, pp. 1162-1178.
2. Van Dyke, Milton D.: The Supersonic Blunt-Body Problem - Review and Extension. *Jour. Aero/Space Sci.*, vol. 25, no. 8, Aug. 1958, pp. 485-496.
3. Garabedian, P. R., and Lieberstein, H. M.: On the Numerical Calculation of Detached Bow Shock Waves in Hypersonic Flow. *Jour. Aero. Sci.*, vol. 25, no. 2, Feb. 1958, pp. 109-118.
4. Zlotnick, Martin, and Newman, Donald J.: Theoretical Calculation of the Flow on Blunt-Nosed Axisymmetric Bodies in a Hypersonic Stream. RAD-TR-2-57-29 (Contract No. AF-04(645)-30), AVCO Res. and Advanced Dev. Div., Sept. 19, 1957.
5. Fay, J. A., and Riddell, F. R.: Theory of Stagnation Point Heat Transfer in Dissociated Air. *Jour. Aero. Sci.*, vol. 25, no. 2, Feb. 1958, pp. 73-85, 121.
6. Lees, Lester: Laminar Heat Transfer Over Blunt-Nosed Bodies at Hypersonic Flight Speeds. *Jet Propulsion*, vol. 26, no. 4, Apr. 1956, pp. 259-269.
7. Kemp, Nelson H., Rose, Peter H., and Detra, Ralph W.: Laminar Heat Transfer Around Blunt Bodies in Dissociated Air. Res. Rep. 15, AVCO Res. Lab., May 1958.
8. Van Driest, E. R.: The Problem of Aerodynamic Heating. *Aero. Eng. Rev.*, vol. 15, no. 10, Oct. 1956, pp. 26-41.
9. Rose, Peter H., Probst, Ronald F., and Adams, Mac C.: Turbulent Heat Transfer Through a Highly Cooled Partially Dissociated Boundary Layer. Res. Rep. 14, AVCO Res. Lab., Jan. 1958.
10. Libby, Paul A., and Cresci, Robert J.: Evaluation of Several Hypersonic Turbulent Heat Transfer Analyses by Comparison With Experimental Data. WADC Tech. Note 57-72, ASTIA Doc. No. AD 118093, U. S. Air Force, July 1957.
11. Tetervin, Neal: Theoretical Distribution of Laminar-Boundary-Layer Thickness, Boundary-Layer Reynolds Number and Stability Limit, and Roughness Reynolds Number for a Sphere and Disk in Incompressible Flow. NACA TN 4350, 1958.

L-115

12. Chauvin, Leo T., and Maloney, Joseph P.: Experimental Convective Heat Transfer to a 4-Inch and 6-Inch Hemisphere at Mach Numbers From 1.62 to 3.04. NACA RM L53L08a, 1954.
13. Cooper, Morton, and Mayo, Edward E.: Normal Conduction Effects on Heat-Transfer Data During Transient Heating of Thin-Skin Models. Jour. Aero. Sci. (Readers' Forum), vol. 24, no. 6, June 1957, pp. 461-462.
14. Carslaw, H. S., and Jaeger, J. C.: Conduction of Heat in Solids. The Clarendon Press (Oxford), 1947, pp. 258-259.
15. Trimpi, Robert L., and Jones, Robert A.: Transient Temperature Distribution in a Two-Component Semi-Infinite Composite Slab of Arbitrary Materials Subjected to Aerodynamic Heating With a Discontinuous Change in Equilibrium Temperature or Heat-Transfer Coefficient. NACA TN 4308, 1958.
16. Ivey, H. Reese, Klunker, E. Bernard, and Bowen, Edward N.: A Method for Determining the Aerodynamic Characteristics of Two- and Three-Dimensional Shapes at Hypersonic Speeds. NACA TN 1613, 1948.
17. Maslen, Stephen H., and Moeckel, W. E.: Inviscid Hypersonic Flow Past Blunt Bodies. Jour. Aero. Sci., vol. 24, no. 9, Sept. 1957, pp. 683-693.
18. Winkler, E. M., and Danberg, J. E.: Heat-Transfer Characteristics of a Hemisphere Cylinder at Hypersonic Mach Numbers. NAVORD Rep. 4259 (Aeroballistic Res. Rep. 336), U. S. Naval Ord. Lab. (White Oak, Md.), Apr. 11, 1957.
19. Stine, Howard A., and Wanlass, Kent: Theoretical and Experimental Investigation of Aerodynamic-Heating and Isothermal Heat-Transfer Parameters on a Hemispherical Nose With Laminar Boundary Layer at Supersonic Mach Numbers. NACA TN 3344, 1954.
20. Crawford, Davis H., and McCauley, William D.: Investigation of the Laminar Aerodynamic Heat-Transfer Characteristics of a Hemisphere-Cylinder in the Langley 11-Inch Hypersonic Tunnel at a Mach Number of 6.8. NACA Rep. 1323, 1957. (Supersedes NACA TN 3706.)
21. Oliver, Robert E.: An Experimental Investigation of Flow Over Simple Blunt Bodies at a Nominal Mach Number of 5.8. GALCIT Memo. No. 26 (Contract No. DA-04-495-Ord-19), June 1, 1955.
22. Diaconis, N. S., Wisniewski, Richard J., and Jack, John R.: Heat Transfer and Boundary-Layer Transition on Two Blunt Bodies at Mach Number 3.12. NACA TN 4099, 1957.

23. Korobkin, Irving: Local Flow Conditions, Recovery Factors and Heat-Transfer Coefficients on the Nose of a Hemisphere-Cylinder at a Mach Number of 2.8. NAVORD Rep. 2865 (Aeroballistic Res. Rep. 175), U. S. Naval Ord. Lab. (White Oak, Md.), May 5, 1953.
24. Boison, J. C., and Curtiss, H. A.: Preliminary Results of Spherical-Segment Blunt Body Pressure Surveys in the 20 Inch Supersonic Wind Tunnel at JPL. RAD Tech. Memo 2-TM-57-77 (Aerod. Sec. Memo. No. 152), AVCO Res. and Advanced Dev. Div., Oct. 9, 1957.
25. Probstein, Ronald F.: Inviscid Flow in the Stagnation Point Region of Very Blunt-Nosed Bodies at Hypersonic Flight Speeds. WADC TN 56-395 (Contract No. AF 33(616)-2798), U. S. Air Force, Sept. 1956. (Available from ASTIA as Doc. No. AD97273.)
26. Milne-Thomson, L. M.: Theoretical Hydrodynamics. Second ed., The Macmillan Co., 1950, pp. 423-425.
27. Beckwith, Ivan E.: The Effect of Gas Properties on the Heat Transfer in Stagnation Flows. Jour. Aero/Space Sci. (Readers' Forum), vol. 25, no. 8, Aug. 1958, pp. 533-534.
28. Hansen, C. Frederick: Approximations for the Thermodynamic and Transport Properties of High-Temperature Air. NACA TN 4150, 1958.

TABLE I.- EXPERIMENTAL PRESSURE RATIOS p/p_t FOR THE SIX BLUNT BODIES

(a) Model with $C_b = 0.546$

$\frac{s}{R}$	Values of p/p_t at -		
	$P_{t,\infty} = 620$ lb/sq in.; $T_{t,\infty} = 375^\circ$ F; $N_{Re,D} = 3.3 \times 10^6$	$P_{t,\infty} = 1,525$ lb/sq in.; $T_{t,\infty} = 375^\circ$ F; $N_{Re,D} = 8.0 \times 10^6$	$P_{t,\infty} = 2,475$ lb/sq in.; $T_{t,\infty} = 370^\circ$ F; $N_{Re,D} = 13.2 \times 10^6$
	0	1.0	1.0
.250	.982	.997	.991
.440	.976	.970	.967
.575	.950	.942	.933
.690	.875	.887	.879
.805	.799	.812	.801
.920	.674	.681	.671

(b) Model with $C_b = 0.586$

$\frac{s}{R}$	Values of p/p_t at -		
	$P_{t,\infty} = 615$ lb/sq in.; $T_{t,\infty} = 370^\circ$ F; $N_{Re,D} = 3.3 \times 10^6$	$P_{t,\infty} = 1,520$ lb/sq in.; $T_{t,\infty} = 380^\circ$ F; $N_{Re,D} = 7.9 \times 10^6$	$P_{t,\infty} = 2,510$ lb/sq in.; $T_{t,\infty} = 390^\circ$ F; $N_{Re,D} = 12.9 \times 10^6$
	0	1.0	1.0
.378	.974	.971	.966
.567	.877	.905	.900
.756	.756	.743	.740
.861	.582	.596	.595
.946	.499	.471	.465
1.040	.268	.267	.266

(c) Model with $C_b = 0.596$

$\frac{s}{R}$	Values of p/p_t at -					
	$P_{t,\infty} = 615$ lb/sq in.; $T_{t,\infty} = 370^\circ$ F; $N_{Re,D} = 3.3 \times 10^6$	$P_{t,\infty} = 1,520$ lb/sq in.; $T_{t,\infty} = 375^\circ$ F; $N_{Re,D} = 8.0 \times 10^6$	$P_{t,\infty} = 2,505$ lb/sq in.; $T_{t,\infty} = 375^\circ$ F; $N_{Re,D} = 13.3 \times 10^6$	$P_{t,\infty} = 620$ lb/sq in.; $T_{t,\infty} = 370^\circ$ F; $N_{Re,D} = 3.3 \times 10^6$	$P_{t,\infty} = 1,520$ lb/sq in.; $T_{t,\infty} = 385^\circ$ F; $N_{Re,D} = 7.9 \times 10^6$	$P_{t,\infty} = 2,515$ lb/sq in.; $T_{t,\infty} = 381^\circ$ F; $N_{Re,D} = 13.0 \times 10^6$
	0	1.0	1.0	1.0	1.0	1.0
.141	.990	1.000	.997	.992	.998	.997
.282	.984	.989	.987	.982	.987	.987
.423	.961	.966	.964	.955	.962	.966
.564	.908	.924	.921	.913	.922	.924
.705	.840	.848	.849	.842	.847	.851
.846	.751	.760	.754	.756	.760	.755
.987	.591	.596	.581	.580	.586	.581

(d) Model with $C_b = 0.597$

$\frac{s}{R}$	Values of p/p_t at -		
	$P_{t,\infty} = 620$ lb/sq in.; $T_{t,\infty} = 375^\circ$ F; $N_{Re,D} = 3.3 \times 10^6$	$P_{t,\infty} = 1,515$ lb/sq in.; $T_{t,\infty} = 380^\circ$ F; $N_{Re,D} = 7.9 \times 10^6$	$P_{t,\infty} = 2,495$ lb/sq in.; $T_{t,\infty} = 375^\circ$ F; $N_{Re,D} = 13.1 \times 10^6$
	0	1.0	1.0
.255	.987	.989	.984
.470	.968	.918	.914
.705	.749	.749	.746
.823	.613	.629	.625
.940	.460	.477	.468
1.058	.285	.296	.293

(e) Hemispherical-nosed model

$\frac{s}{R}$	Values of p/p_t at -		
	$P_{t,\infty} = 615$ lb/sq in.; $T_{t,\infty} = 376^\circ$ F; $N_{Re,D} = 3.2 \times 10^6$	$P_{t,\infty} = 1,515$ lb/sq in.; $T_{t,\infty} = 375^\circ$ F; $N_{Re,D} = 8.0 \times 10^6$	$P_{t,\infty} = 2,505$ lb/sq in.; $T_{t,\infty} = 380^\circ$ F; $N_{Re,D} = 13.0 \times 10^6$
	0	1.0	1.0
.174	.969	.972	.971
.349	.874	.890	.891
.524	.750	.763	.764
.698	.580	.597	.596
.960	.328	.344	.342
1.222	.114	.166	.168
1.483	.069	.069	.069

(f) Flat-nosed model^a

$\frac{s}{R}$	Values of p/p_t at -					
	$P_{t,\infty} = 625$ lb/sq in.; $T_{t,\infty} = 370^\circ$ F; $N_{Re,D} = 3.3 \times 10^6$	$P_{t,\infty} = 1,515$ lb/sq in.; $T_{t,\infty} = 365^\circ$ F; $N_{Re,D} = 8.1 \times 10^6$	$P_{t,\infty} = 2,510$ lb/sq in.; $T_{t,\infty} = 365^\circ$ F; $N_{Re,D} = 13.5 \times 10^6$	$P_{t,\infty} = 615$ lb/sq in.; $T_{t,\infty} = 375^\circ$ F; $N_{Re,D} = 3.2 \times 10^6$	$P_{t,\infty} = 1,525$ lb/sq in.; $T_{t,\infty} = 378^\circ$ F; $N_{Re,D} = 7.9 \times 10^6$	$P_{t,\infty} = 2,477$ lb/sq in.; $T_{t,\infty} = 375^\circ$ F; $N_{Re,D} = 13.0 \times 10^6$
	0	1.0	1.0	1.0	1.0	1.0
.25	.992	.999	.996	.995	1.000	.999
.50	.990	.989	.987	.990	.993	.989
.75	.974	.958	.948	.964	.970	.961
.875	.908	.912	.905	.925	.926	.922
.906	.883	.888	.874	.900	.916	.908
.938	.865	.861	.849	.856	.854	.843
.969	.822	.813	.802	.823	.816	.808

^aThese data for flat-nosed model were obtained on pressure gages.

TABLE II.- PRESSURE DISTRIBUTION $\frac{P_t - P}{P_t}$ ON FLAT-NOSED MODEL^a

$$\left[T_{t,\infty} \approx 370^\circ \text{F} \right]$$

Orifice location	S R	$\frac{P_t - P}{P_t}$ for values of $P_{t,\infty}$ of -																
		.15 lb/sq in.	.420 lb/sq in.	.615 lb/sq in.	.615 lb/sq in.	1.015 lb/sq in.	1.020 lb/sq in.	1.515 lb/sq in.	4.15 lb/sq in.	615 lb/sq in.	1,020 lb/sq in.							
Up	0	0	0	0	0	0	0	0	0	0	0	0	0	0	0	0	0	0
	.25	.00313	.0110	.00825	.00699	.00825	.00726	.00567	.00567	.00567	.00567	.00567	.00567	.00567	.00567	.00567	.00567	.00567
	.50	.0267	.0264	.0248	.0247	.0248	.0214	.0201	.0201	.0201	.0201	.0201	.0201	.0201	.0201	.0201	.0201	.0201
Down	0	0	0	0	0	0	0	0	0	0	0	0	0	0	0	0	0	0
	.25	.0678	.0642	.0629	.0622	.0622	.0602	.0576	.0576	.0576	.0576	.0576	.0576	.0576	.0576	.0576	.0576	.0576
	.50	.0678	.0642	.0629	.0622	.0622	.0602	.0576	.0576	.0576	.0576	.0576	.0576	.0576	.0576	.0576	.0576	.0576
Up	0	0	0	0	0	0	0	0	0	0	0	0	0	0	0	0	0	0
	.25	.00607	.0110	.00695	.00699	.00695	.00726	.00699	.00699	.00699	.00699	.00699	.00699	.00699	.00699	.00699	.00699	.00699
	.50	.0236	.0264	.0244	.0247	.0244	.0214	.0247	.0247	.0247	.0247	.0247	.0247	.0247	.0247	.0247	.0247	.0247
Down	0	0	0	0	0	0	0	0	0	0	0	0	0	0	0	0	0	0
	.25	.00364	.0110	.00512	.00500	.00512	.00500	.00482	.00482	.00482	.00482	.00482	.00482	.00482	.00482	.00482	.00482	.00482
	.50	.0201	.0264	.0202	.0206	.0202	.0206	.0215	.0215	.0215	.0215	.0215	.0215	.0215	.0215	.0215	.0215	.0215

^aThese data for flat-nosed model were obtained on butyl phthalate manometer.

TABLE III.- EXPERIMENTAL HEAT-TRANSFER COEFFICIENTS h FOR 0.050 MODELS^a(a) Model with $C_3 = 0.597$

$\frac{h}{R}$	Values of h , Btu/(sq ft)(sec)(°F), at -	
	$P_{t,\infty} = 1,015$ lb/sq in.; $T_{t,\infty} = 401^\circ$ F; $N_{Re,D} = 5.1 \times 10^6$; test 44	$P_{t,\infty} = 1,015$ lb/sq in.; $T_{t,\infty} = 397^\circ$ F; $N_{Re,D} = 5.2 \times 10^6$; test 45
0	0.0480	0.0450
.235	.0467	.0465
.470	.0477	.0482
.705	.0471	.0475
.823	.0408	.0414
.940	.0339	.0358
1.058	.0300	.0286
1.175	.0286	.0256

(b) Model with $C_4 = 0.586$

$\frac{h}{R}$	Values of h , Btu/(sq ft)(sec)(°F), at -				
	$P_{t,\infty} = 1,015$ lb/sq in.; $T_{t,\infty} = 404^\circ$ F; $N_{Re,D} = 5.1 \times 10^6$; test 46	$P_{t,\infty} = 1,515$ lb/sq in.; $T_{t,\infty} = 397^\circ$ F; $N_{Re,D} = 7.7 \times 10^6$; test 47	$P_{t,\infty} = 2,530$ lb/sq in.; $T_{t,\infty} = 393^\circ$ F; $N_{Re,D} = 12.9 \times 10^6$; test 48	$P_{t,\infty} = 1,515$ lb/sq in.; $T_{t,\infty} = 706^\circ$ F; $N_{Re,D} = 4.8 \times 10^6$; test 52	$P_{t,\infty} = 2,545$ lb/sq in.; $T_{t,\infty} = 715^\circ$ F; $N_{Re,D} = 7.9 \times 10^6$; test 53
0	0.0422	0.0467	0.0532	0.0530	0.0594
.378	.0422	.0454	.0544	.0529	.0644
.567	.0426	.0457	b .0636	.0550	b .0715
.756	.0392	.0439	b .0763	.0509	b .0799
.891	.0366	.0426	b .0811	.0492	b .0891
.946	.0301	.0333	b .0748	.0398	b .0735
1.040	.0266	.0323	b .0734	.0340	b .0777
1.135	.0223	.0261	b,c .0778	.0304	b,d .0607

(c) Hemispherical-nosed model

$\frac{h}{R}$	Values of h , Btu/(sq ft)(sec)(°F), at -				
	$P_{t,\infty} = 1,010$ lb/sq in.; $T_{t,\infty} = 395^\circ$ F; $N_{Re,D} = 5.1 \times 10^6$; test 3	$P_{t,\infty} = 1,515$ lb/sq in.; $T_{t,\infty} = 400^\circ$ F; $N_{Re,D} = 7.6 \times 10^6$; test 42	$P_{t,\infty} = 2,525$ lb/sq in.; $T_{t,\infty} = 396^\circ$ F; $N_{Re,D} = 12.9 \times 10^6$; test 43	$P_{t,\infty} = 1,015$ lb/sq in.; $T_{t,\infty} = 400^\circ$ F; $N_{Re,D} = 5.1 \times 10^6$; test 49	$P_{t,\infty} = 1,015$ lb/sq in.; $T_{t,\infty} = 692^\circ$ F; $N_{Re,D} = 3.2 \times 10^6$; test 50
0	.047	0.0560	0.0681	0.0607	-----
.174	-----	-----	-----	-----	-----
.349	-----	-----	-----	-----	-----
.523	.0450	.0500	.0632	.0436	0.0483
.698	.0329	.0411	.0504	.0375	.0382
.960	.0230	.0177	.0237	.0202	.0200
1.222	.0153	.0169	.0208	.0158	.0170
1.483	.0082	.0080	.0092	.0097	.0103

(d) Flat-nosed model^e

$\frac{h}{R}$	Values of h , Btu/(sq ft)(sec)(°F), at -				
	$P_{t,\infty} = 1,520$ lb/sq in.; $T_{t,\infty} = 398^\circ$ F; $N_{Re,D} = 7.7 \times 10^6$; test 34	$P_{t,\infty} = 2,515$ lb/sq in.; $T_{t,\infty} = 396^\circ$ F; $N_{Re,D} = 12.8 \times 10^6$; test 35	$P_{t,\infty} = 1,513$ lb/sq in.; $T_{t,\infty} = 396^\circ$ F; $N_{Re,D} = 7.7 \times 10^6$; test 39	$P_{t,\infty} = 1,515$ lb/sq in.; $T_{t,\infty} = 725^\circ$ F; $N_{Re,D} = 4.6 \times 10^6$; test 51	$P_{t,\infty} = 2,535$ lb/sq in.; $T_{t,\infty} = 694^\circ$ F; $N_{Re,D} = 8.0 \times 10^6$; test 54
0	0.0294	0.0402	0.0290	0.0385	0.0475
.240	.0365	.0502	.0392	.0430	.0618
.500	.0385	.0594	.0452	.0473	.0688
.750	.0418	.0788	.0503	.0564	.0750
.875	.0582	.0943	.0554	.0557	.0820
.906	.0526	.1010	.0536	.0590	.0866
.938	.0523	.0972	.0542	.0544	.0810
.969	.0421	.0813	.0470	.0470	.0686

^aAll values based on laminar recovery factor unless otherwise specified.^bValues based on turbulent recovery factor.^cValues would be 11 percent higher if laminar recovery factor were used.^dValues would be 7 percent higher if laminar recovery factor were used.^eNo significant difference if turbulent recovery factor used.

TABLE IV.- EXPERIMENTAL HEAT-TRANSFER COEFFICIENTS h FOR 0.060 MODELS

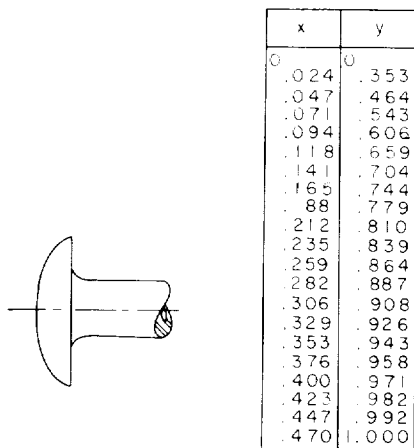
(a) Hemispherical-nosed model

$\frac{s}{R}$	Values of h , Btu/(sq ft)(sec)($^{\circ}$ F), at -		
	$p_{t,\infty} = 2,475$ lb/sq in.; $T_{t,\infty} = 417^{\circ}$ F; $N_{Re,D} = 12.1 \times 10^6$; test 56	$p_{t,\infty} = 2,490$ lb/sq in.; $T_{t,\infty} = 413^{\circ}$ F; $N_{Re,D} = 12.3 \times 10^6$; test 57	$p_{t,\infty} = 1,025$ lb/sq in.; $T_{t,\infty} = 408^{\circ}$ F; $N_{Re,D} = 5.1 \times 10^6$; test 58
0	0.0821	0.0913	0.0614
.174	.0803	.0823	.0579
.349	.0579	^a .0706	.0514
.524	-----	-----	-----
.698	.0514	^a .1316	.0405
.873	.0406	^a .1231	.0334
1.047	.0416	^a .1254	.0320
1.222	.0394	^a .0826	.0423
1.396	.0131	^a .0462	.0223
1.571	.0105	^a .0305	.0127
1.047	^{a,b} .0835		

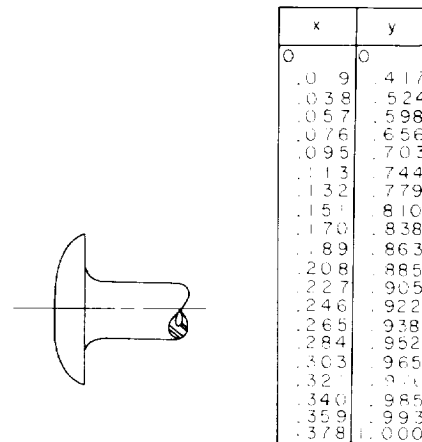
(b) Flat-nosed model^a

$\frac{s}{R}$	Values of h , Btu/(sq ft)(sec)($^{\circ}$ F), at -		
	$p_{t,\infty} = 2,475$ lb/sq in.; $T_{t,\infty} = 431^{\circ}$ F; $N_{Re,D} = 11.8 \times 10^6$; test 60	$p_{t,\infty} = 2,435$ lb/sq in.; $T_{t,\infty} = 406^{\circ}$ F; $N_{Re,D} = 12.4 \times 10^6$; test 61	$p_{t,\infty} = 2,445$ lb/sq in.; $T_{t,\infty} = 395^{\circ}$ F; $N_{Re,D} = 12.7 \times 10^6$; test 63
0	0.0656	0.0607	-----
.125	.0638	.0607	0.0676
.250	.0802	.0690	-----
.375	.0815	.0733	.0715
.500	.0856	.0753	.0712
.563	.1088	.0866	.0828
.625	.0944	.0857	.0861
.688	.0980	.0975	.0968
.750	.1078	.1045	.1023
.813	.1018	.1081	.1151
.875	.1162	.1227	.1287

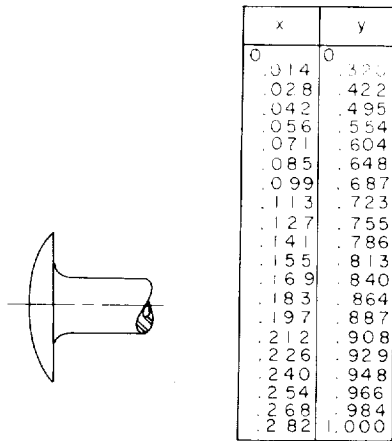
^aValues based on turbulent recovery factor^bValue obtained 0.7 second after obtaining other data of test 56.



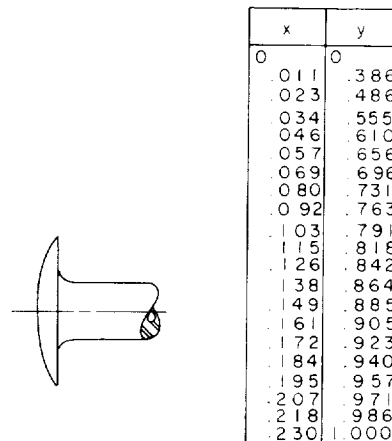
$C_3 = .597$



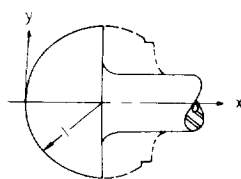
$C_4 = .586$



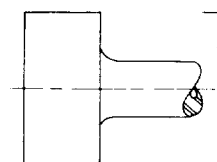
$C_3 = .356$



$C_4 = .346$



Hemisphere



Flat nose

Figure 1.- Geometry of blunt-nosed models. All dimensions are in inches.

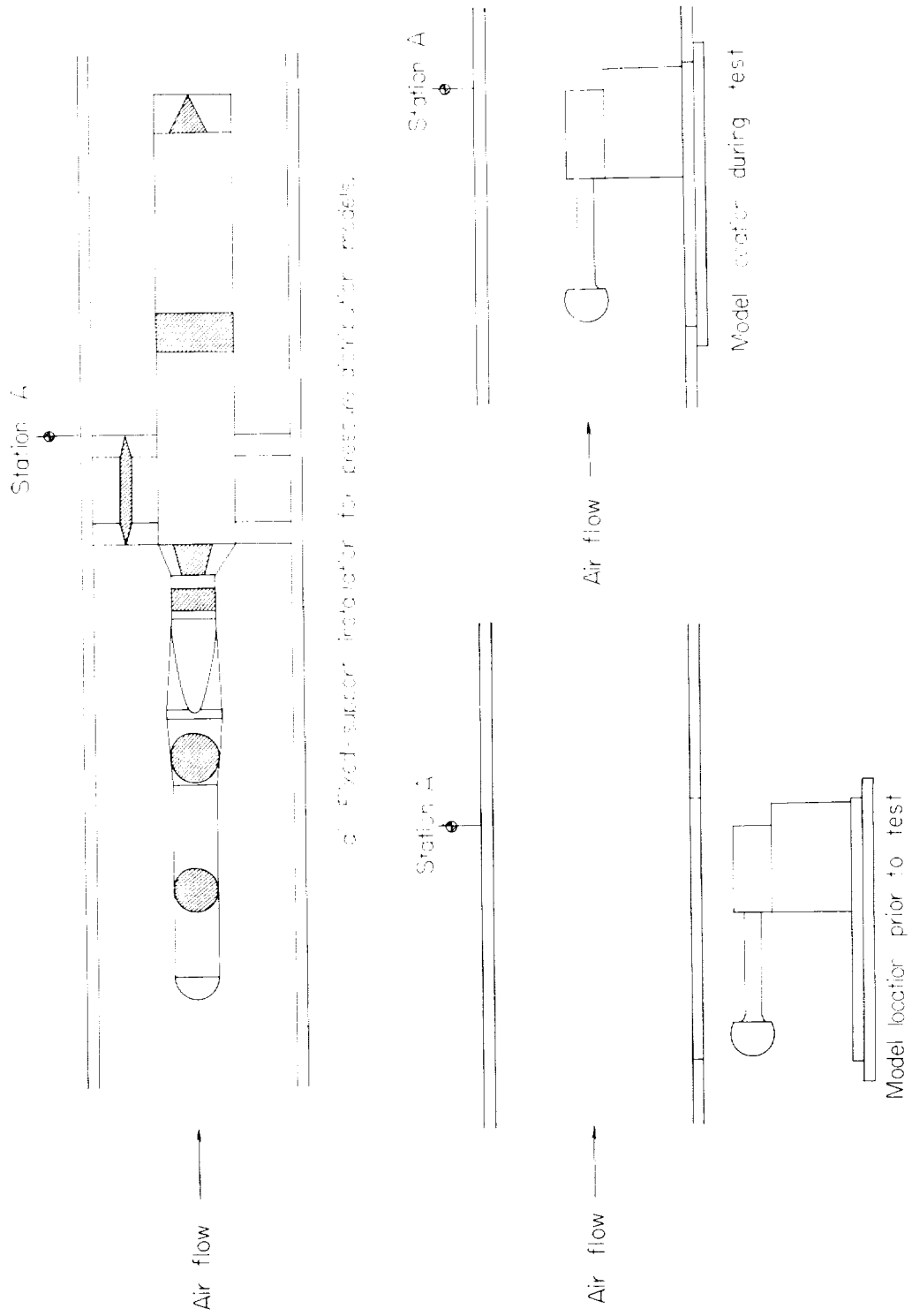


Figure 2.- Typical model installations.

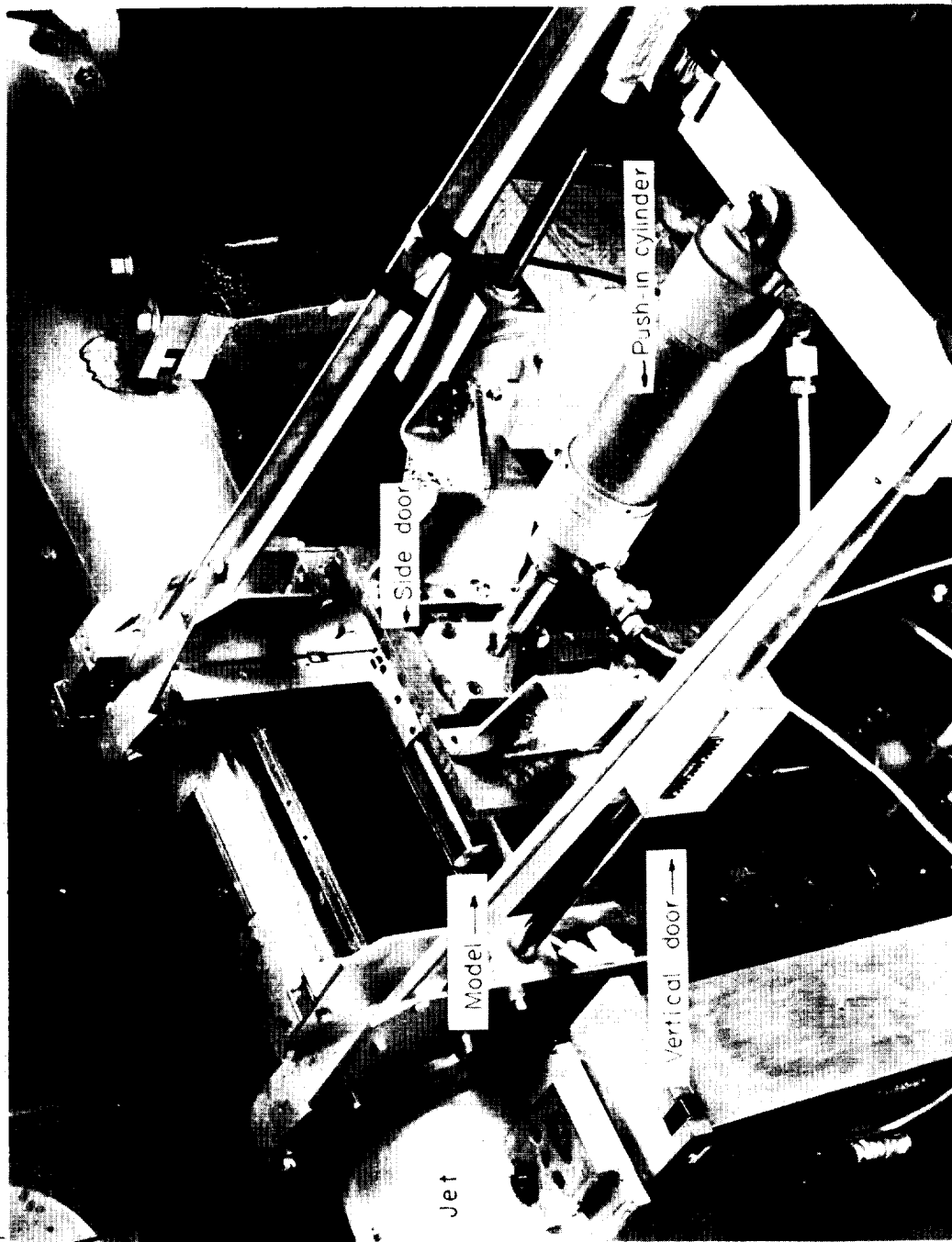


Figure 3.- Photograph of push-in side-support installation for heat-transfer model. L-57-2907.1

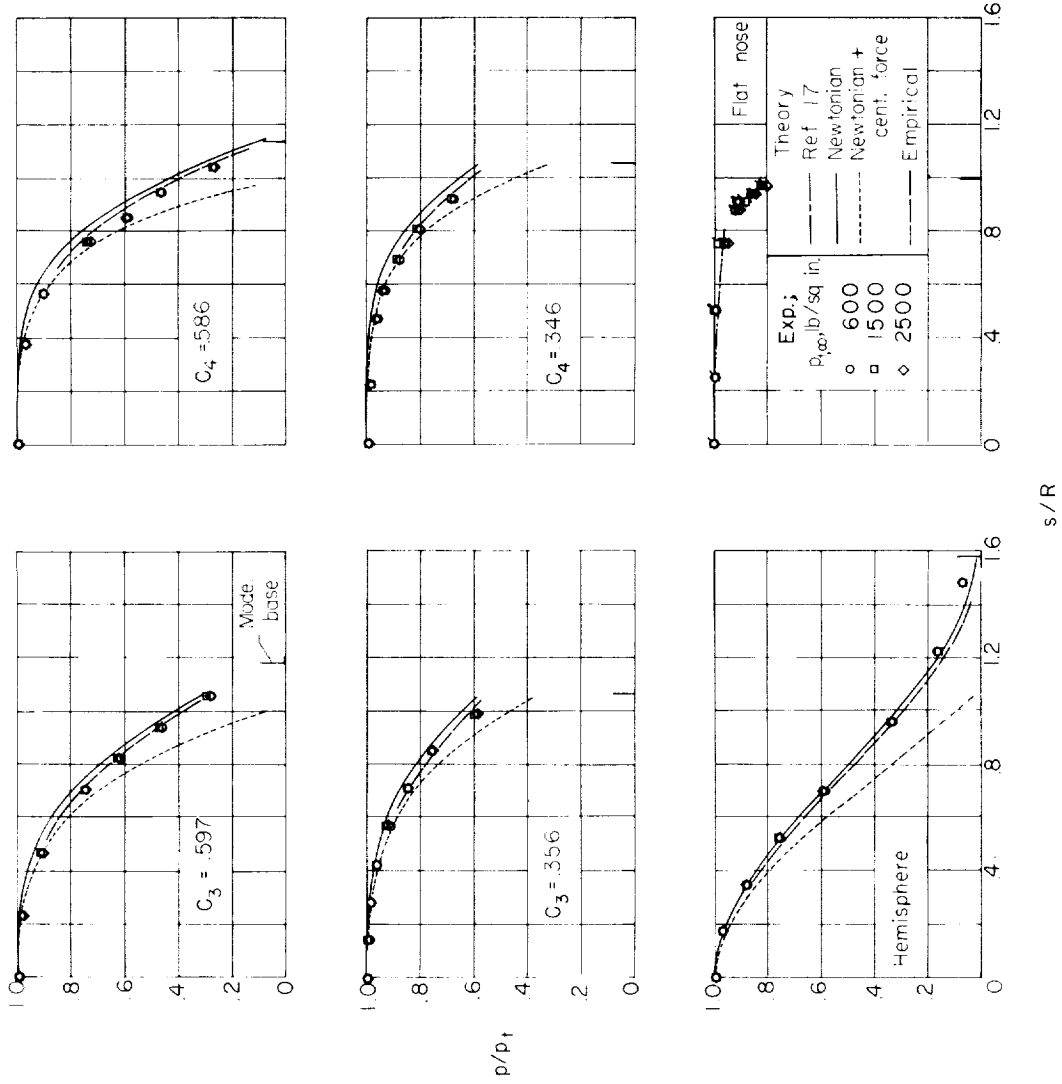
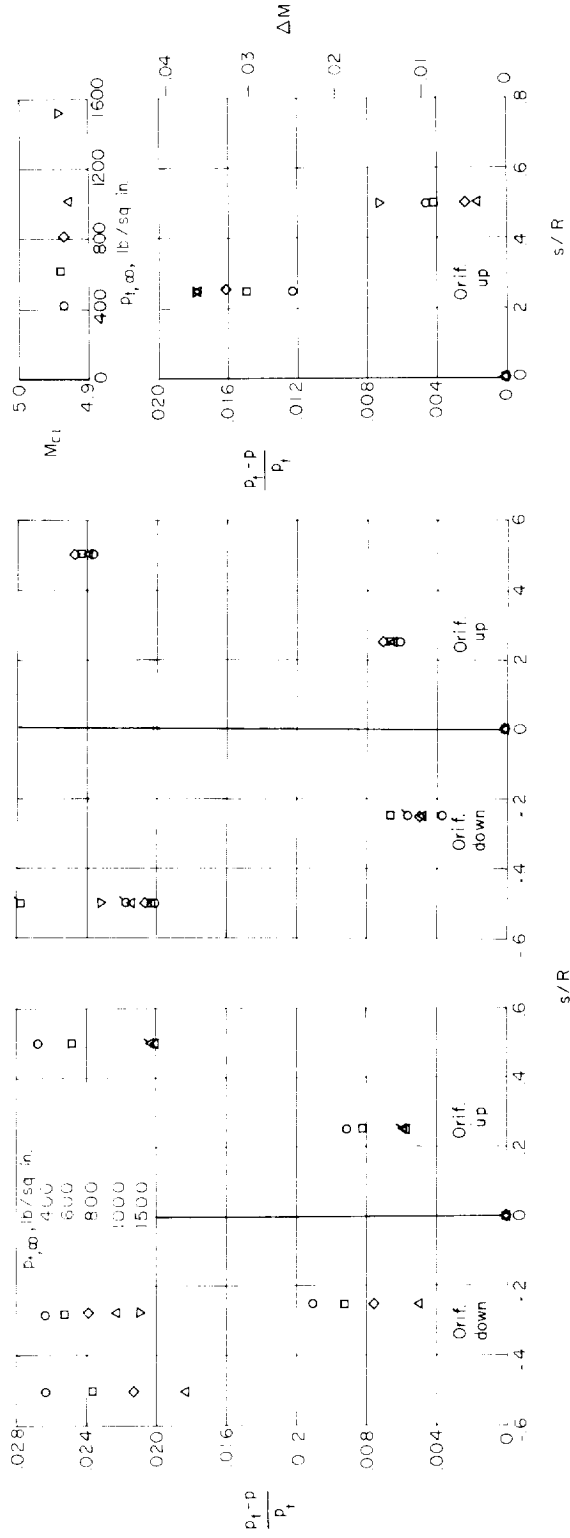


Figure 4.- Comparison of experimental and theoretical pressure distributions. $T_{t,\infty} \approx 375^\circ \text{F}$; flagged symbols indicate repeat tests.



(a) Model located on jet center line.
 (b) Model located 1 inch from jet center line.
 (c) Survey rake located on jet center line.

Figure 5.- Pressure distributions on flat-nosed model and corresponding jet-empty survey. Flagged symbols indicate repeat tests.

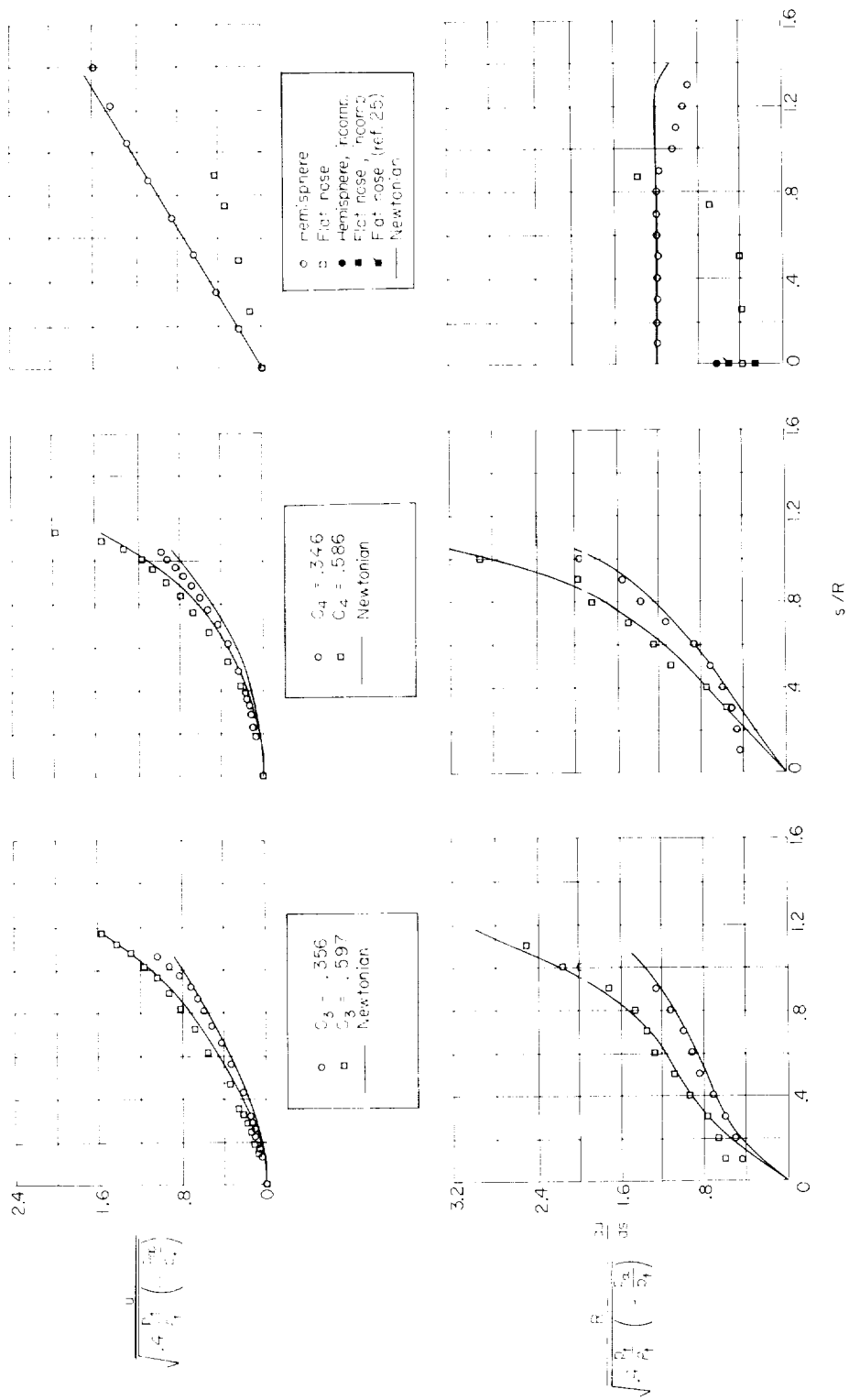
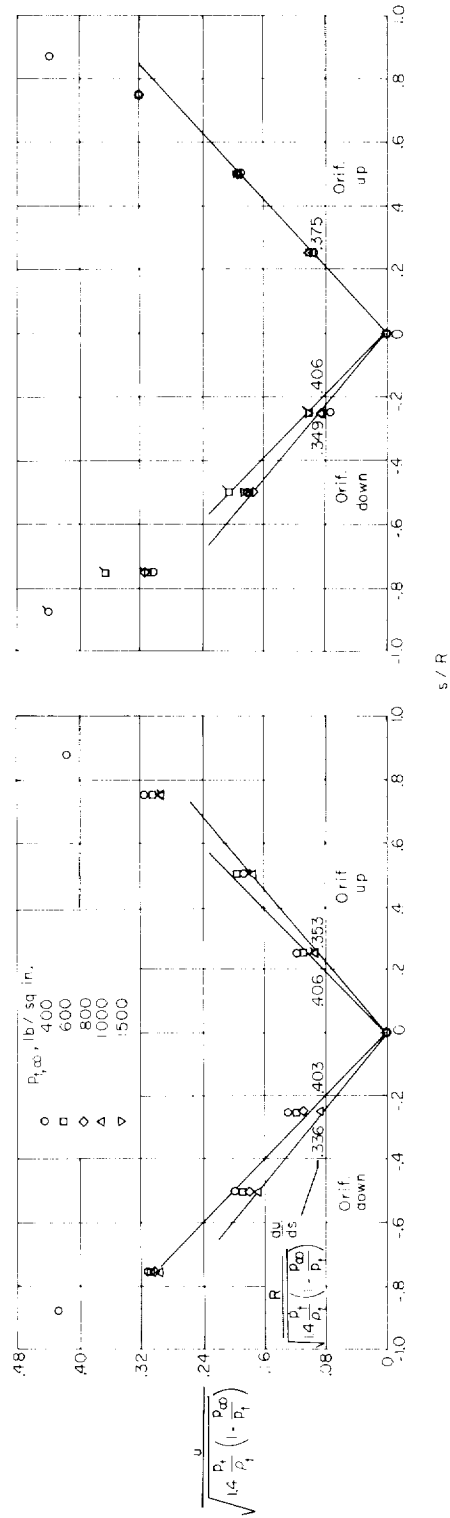


Figure 6.- Comparison of experimental velocity and velocity-gradient distributions with theory. Solid symbols represent theoretical points.



(a) Model located on jet center line.

(b) Model located 1 inch from jet center line.

Figure 7.- Velocity distribution on flat-nosed model. Flagged symbols indicate repeat tests.

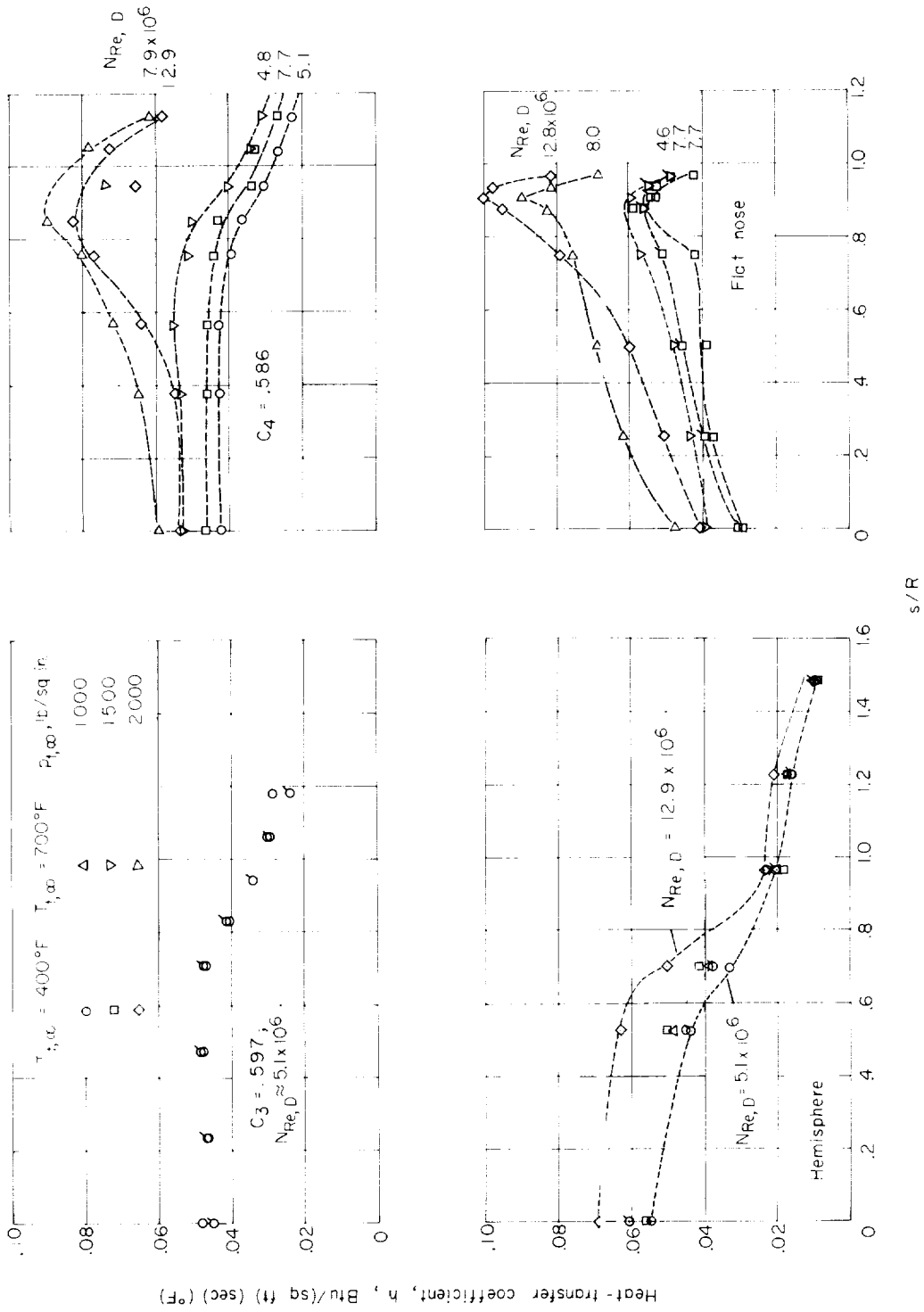
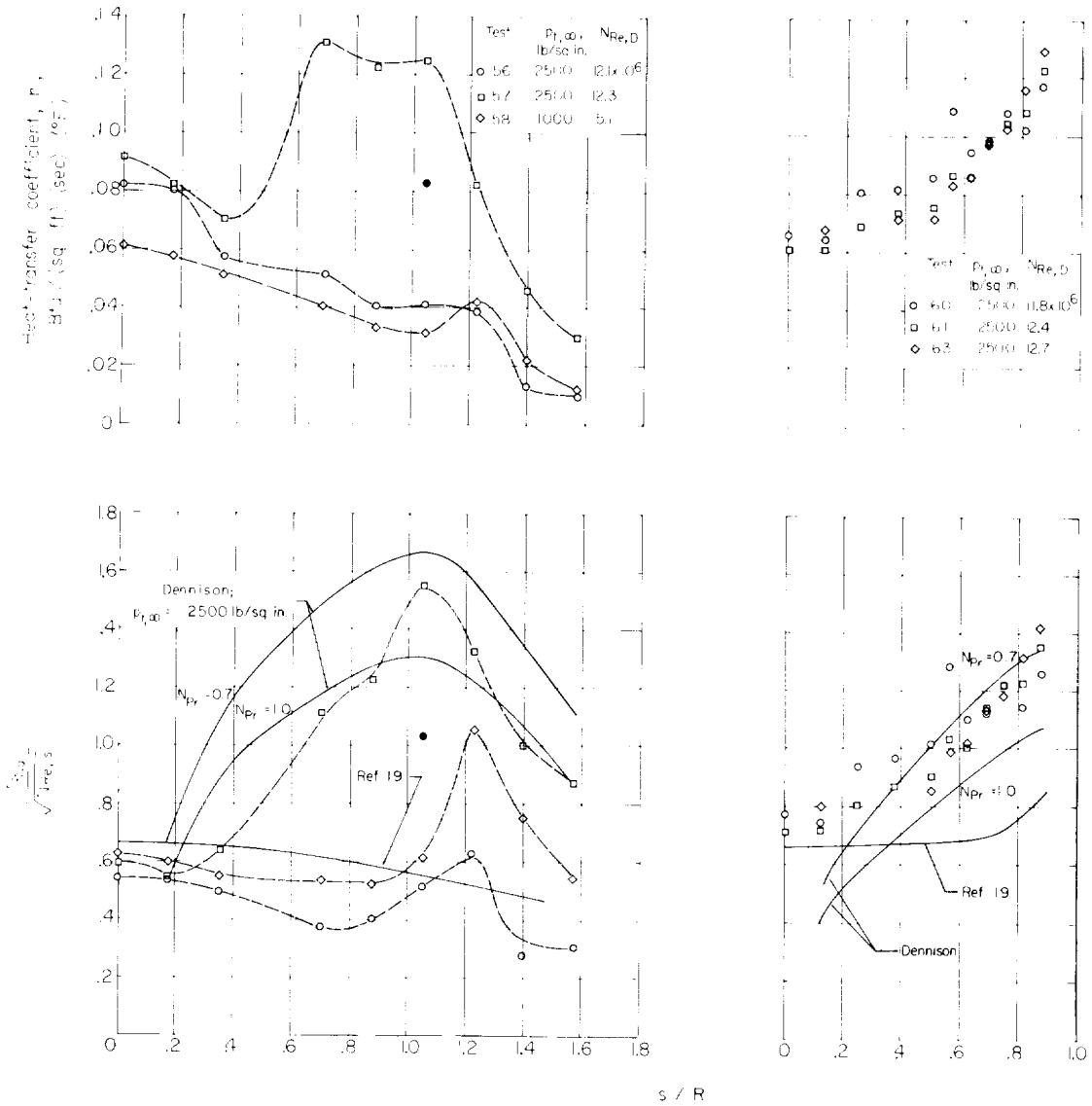


Figure 8.- Heat-transfer coefficients for four blunt-nosed models. $\tau = 0.030$ inch; flagged symbols indicate repeat tests.



(a) Hemispherical nose.

(b) Flat nose.

Figure 9.- Comparison of experimental and theoretical heat transfer on hemispherical- and flat-nosed models. $\tau = 0.060$ inch; $T_{t,\infty} = 400^\circ\text{F}$; solid symbols indicate data obtained 0.7 second after obtaining other data of same test.

<p>NASA MEMO 1-3-59L National Aeronautics and Space Administration. MEASUREMENTS OF LOCAL HEAT TRANSFER AND PRESSURE ON SIX 2-INCH-DIAMETER BLUNT BODIES AT A MACH NUMBER OF 4.95 AND AT REYNOLDS NUMBERS PER FOOT UP TO 81×10^6. Morton Cooper and Edward E. Mayo. March 1959. 39p. diags., photo., tabs. (NASA MEMORANDUM 1-3-59L)</p> <p>Laminar flow was observed over a hemispherical-nosed body having a surface finish from 10 to 20 microinches at the highest test Reynolds number per foot (for this configuration) of 77.4×10^6. The pressures measured on the hemisphere agreed very well with those of the modified Newtonian theory, whereas the pressures on all other bodies, except on the flat-nosed body, were bracketed by those of the modified Newtonian theory both with and without centrifugal forces. Heat-transfer results were compared with those of laminar- and turbulent-flow theories.</p>	<p>NASA MEMO 1-3-59L National Aeronautics and Space Administration. MEASUREMENTS OF LOCAL HEAT TRANSFER AND PRESSURE ON SIX 2-INCH-DIAMETER BLUNT BODIES AT A MACH NUMBER OF 4.95 AND AT REYNOLDS NUMBERS PER FOOT UP TO 81×10^6. Morton Cooper and Edward E. Mayo. March 1959. 39p. diags., photo., tabs. (NASA MEMORANDUM 1-3-59L)</p> <p>Laminar flow was observed over a hemispherical-nosed body having a surface finish from 10 to 20 microinches at the highest test Reynolds number per foot (for this configuration) of 77.4×10^6. The pressures measured on the hemisphere agreed very well with those of the modified Newtonian theory, whereas the pressures on all other bodies, except on the flat-nosed body, were bracketed by those of the modified Newtonian theory both with and without centrifugal forces. Heat-transfer results were compared with those of laminar- and turbulent-flow theories.</p>	<p>1. Flow, Laminar (1.1.3.1) 2. Flow, Turbulent (1.1.3.2) 3. Heat Transfer, Aerodynamic (1.1.4.2) 4. Bodies - Thickness Distribution (1.3.2.3) 5. Bodies - Surface Conditions (1.3.2.4) I. Cooper, Morton II. Mayo, Edward E. III. NASA MEMO 1-3-59L</p>	<p>1. Flow, Laminar (1.1.3.1) 2. Flow, Turbulent (1.1.3.2) 3. Heat Transfer, Aerodynamic (1.1.4.2) 4. Bodies - Thickness Distribution (1.3.2.3) 5. Bodies - Surface Conditions (1.3.2.4) I. Cooper, Morton II. Mayo, Edward E. III. NASA MEMO 1-3-59L</p>
<p>NASA MEMO 1-3-59L National Aeronautics and Space Administration. MEASUREMENTS OF LOCAL HEAT TRANSFER AND PRESSURE ON SIX 2-INCH-DIAMETER BLUNT BODIES AT A MACH NUMBER OF 4.95 AND AT REYNOLDS NUMBERS PER FOOT UP TO 81×10^6. Morton Cooper and Edward E. Mayo. March 1959. 39p. diags., photo., tabs. (NASA MEMORANDUM 1-3-59L)</p> <p>Laminar flow was observed over a hemispherical-nosed body having a surface finish from 10 to 20 microinches at the highest test Reynolds number per foot (for this configuration) of 77.4×10^6. The pressures measured on the hemisphere agreed very well with those of the modified Newtonian theory, whereas the pressures on all other bodies, except on the flat-nosed body, were bracketed by those of the modified Newtonian theory both with and without centrifugal forces. Heat-transfer results were compared with those of laminar- and turbulent-flow theories.</p>	<p>NASA MEMO 1-3-59L National Aeronautics and Space Administration. MEASUREMENTS OF LOCAL HEAT TRANSFER AND PRESSURE ON SIX 2-INCH-DIAMETER BLUNT BODIES AT A MACH NUMBER OF 4.95 AND AT REYNOLDS NUMBERS PER FOOT UP TO 81×10^6. Morton Cooper and Edward E. Mayo. March 1959. 39p. diags., photo., tabs. (NASA MEMORANDUM 1-3-59L)</p> <p>Laminar flow was observed over a hemispherical-nosed body having a surface finish from 10 to 20 microinches at the highest test Reynolds number per foot (for this configuration) of 77.4×10^6. The pressures measured on the hemisphere agreed very well with those of the modified Newtonian theory, whereas the pressures on all other bodies, except on the flat-nosed body, were bracketed by those of the modified Newtonian theory both with and without centrifugal forces. Heat-transfer results were compared with those of laminar- and turbulent-flow theories.</p>	<p>1. Flow, Laminar (1.1.3.1) 2. Flow, Turbulent (1.1.3.2) 3. Heat Transfer, Aerodynamic (1.1.4.2) 4. Bodies - Thickness Distribution (1.3.2.3) 5. Bodies - Surface Conditions (1.3.2.4) I. Cooper, Morton II. Mayo, Edward E. III. NASA MEMO 1-3-59L</p>	<p>1. Flow, Laminar (1.1.3.1) 2. Flow, Turbulent (1.1.3.2) 3. Heat Transfer, Aerodynamic (1.1.4.2) 4. Bodies - Thickness Distribution (1.3.2.3) 5. Bodies - Surface Conditions (1.3.2.4) I. Cooper, Morton II. Mayo, Edward E. III. NASA MEMO 1-3-59L</p>

NASA MEMO 1-3-59L
National Aeronautics and Space Administration.
MEASUREMENTS OF LOCAL HEAT TRANSFER
AND PRESSURE ON SIX 2-INCH-DIAMETER BLUNT
BODIES AT A MACH NUMBER OF 4.95 AND AT
REYNOLDS NUMBERS PER FOOT UP TO 81×10^6 .
Morton Cooper and Edward E. Mayo. March 1959.
39p. diags., photo., tabs.
(NASA MEMORANDUM 1-3-59L)

Laminar flow was observed over a hemispherical-nosed body having a surface finish from 10 to 20 microinches at the highest test Reynolds number per foot (for this configuration) of 77.4×10^6 . The pressures measured on the hemisphere agreed very well with those of the modified Newtonian theory, whereas the pressures on all other bodies, except on the flat-nosed body, were bracketed by those of the modified Newtonian theory both with and without centrifugal forces. Heat-transfer results were compared with those of laminar- and turbulent-flow theories.

Copies obtainable from NASA, Washington

1. Flow, Laminar (1.1.3.1)
2. Flow, Turbulent (1.1.3.2)
3. Heat Transfer, Aerodynamic (1.1.4.2)
4. Bodies - Thickness Distribution (1.3.2.3)
5. Bodies - Surface Conditions (1.3.2.4)
- I. Cooper, Morton
- II. Mayo, Edward E.
- III. NASA MEMO 1-3-59L

NASA

NASA MEMO 1-3-59L
National Aeronautics and Space Administration.
MEASUREMENTS OF LOCAL HEAT TRANSFER
AND PRESSURE ON SIX 2-INCH-DIAMETER BLUNT
BODIES AT A MACH NUMBER OF 4.95 AND AT
REYNOLDS NUMBERS PER FOOT UP TO 81×10^6 .
Morton Cooper and Edward E. Mayo. March 1959.
39p. diags., photo., tabs.
(NASA MEMORANDUM 1-3-59L)

Laminar flow was observed over a hemispherical-nosed body having a surface finish from 10 to 20 microinches at the highest test Reynolds number per foot (for this configuration) of 77.4×10^6 . The pressures measured on the hemisphere agreed very well with those of the modified Newtonian theory, whereas the pressures on all other bodies, except on the flat-nosed body, were bracketed by those of the modified Newtonian theory both with and without centrifugal forces. Heat-transfer results were compared with those of laminar- and turbulent-flow theories.

Copies obtainable from NASA, Washington

NASA MEMO 1-3-59L
National Aeronautics and Space Administration.
MEASUREMENTS OF LOCAL HEAT TRANSFER
AND PRESSURE ON SIX 2-INCH-DIAMETER BLUNT
BODIES AT A MACH NUMBER OF 4.95 AND AT
REYNOLDS NUMBERS PER FOOT UP TO 81×10^6 .
Morton Cooper and Edward E. Mayo. March 1959.
39p. diags., photo., tabs.
(NASA MEMORANDUM 1-3-59L)

Laminar flow was observed over a hemispherical-nosed body having a surface finish from 10 to 20 microinches at the highest test Reynolds number per foot (for this configuration) of 77.4×10^6 . The pressures measured on the hemisphere agreed very well with those of the modified Newtonian theory, whereas the pressures on all other bodies, except on the flat-nosed body, were bracketed by those of the modified Newtonian theory both with and without centrifugal forces. Heat-transfer results were compared with those of laminar- and turbulent-flow theories.

Copies obtainable from NASA, Washington

1. Flow, Laminar (1.1.3.1)
2. Flow, Turbulent (1.1.3.2)
3. Heat Transfer, Aerodynamic (1.1.4.2)
4. Bodies - Thickness Distribution (1.3.2.3)
5. Bodies - Surface Conditions (1.3.2.4)
- I. Cooper, Morton
- II. Mayo, Edward E.
- III. NASA MEMO 1-3-59L

NASA

NASA MEMO 1-3-59L
National Aeronautics and Space Administration.
MEASUREMENTS OF LOCAL HEAT TRANSFER
AND PRESSURE ON SIX 2-INCH-DIAMETER BLUNT
BODIES AT A MACH NUMBER OF 4.95 AND AT
REYNOLDS NUMBERS PER FOOT UP TO 81×10^6 .
Morton Cooper and Edward E. Mayo. March 1959.
39p. diags., photo., tabs.
(NASA MEMORANDUM 1-3-59L)

Laminar flow was observed over a hemispherical-nosed body having a surface finish from 10 to 20 microinches at the highest test Reynolds number per foot (for this configuration) of 77.4×10^6 . The pressures measured on the hemisphere agreed very well with those of the modified Newtonian theory, whereas the pressures on all other bodies, except on the flat-nosed body, were bracketed by those of the modified Newtonian theory both with and without centrifugal forces. Heat-transfer results were compared with those of laminar- and turbulent-flow theories.

Copies obtainable from NASA, Washington

1. Flow, Laminar (1.1.3.1)
2. Flow, Turbulent (1.1.3.2)
3. Heat Transfer, Aerodynamic (1.1.4.2)
4. Bodies - Thickness Distribution (1.3.2.3)
5. Bodies - Surface Conditions (1.3.2.4)
- I. Cooper, Morton
- II. Mayo, Edward E.
- III. NASA MEMO 1-3-59L

NASA

1. Flow, Laminar (1.1.3.1)
2. Flow, Turbulent (1.1.3.2)
3. Heat Transfer, Aerodynamic (1.1.4.2)
4. Bodies - Thickness Distribution (1.3.2.3)
5. Bodies - Surface Conditions (1.3.2.4)
- I. Cooper, Morton
- II. Mayo, Edward E.
- III. NASA MEMO 1-3-59L

NASA

